Theses and Dissertations   Thesis and Dissertation Collection

1976

An experimental investigation of the efficiency and experiment rates of a fluidically oscillated jet.

Veltman, Richard James

Monterey, California. Naval Postgraduate School

http://hdl.handle.net/10945/17770

AN EXPERIMENTAL INVESTIGATION
OF THE EFFICIENCY AND ENTRAINMENT RATES
OF A FLUIDICALLY OSCILLATED JET

Richard James Veltman

NAVAL POSTGRADUATE SCHOOL
Monterey, California

THESIS

AN EXPERIMENTAL INVESTIGATION
OF THE EFFICIENCY AND ENTRAINMENT RATES
OF A FLUIDICALLY OSCILLATED JET

by

Richard James Veltman

June 1976

Thesis Advisor: M.F. Platzer

T174980

REPORT DOCUMENTATION PAGE		READ INSTRUCTIONS BEFORE COMPLETING FORM
1. REPORT NUMBER	2. GOVT ACCESSION NO.	3. RECIPIENT'S CATALOG NUMBER
4. TITLE *(and Subtitle)* An Experimental Investigation of the Efficiency and Entrainment Rates of a Fluidically Oscillated Jet		5. TYPE OF REPORT & PERIOD COVERED Master's Thesis; June 1976
		6. PERFORMING ORG. REPORT NUMBER
7. AUTHOR(s) Richard James Veltman		8. CONTRACT OR GRANT NUMBER(s)
9. PERFORMING ORGANIZATION NAME AND ADDRESS Naval Postgraduate School Monterey, California 93940		10. PROGRAM ELEMENT, PROJECT, TASK AREA & WORK UNIT NUMBERS
11. CONTROLLING OFFICE NAME AND ADDRESS Naval Postgraduate School Monterey, California 93940		12. REPORT DATE June 1976
		13. NUMBER OF PAGES 97
14. MONITORING AGENCY NAME & ADDRESS(*if different from Controlling Office*)		15. SECURITY CLASS. *(of this report)* Unclassified
		15a. DECLASSIFICATION/DOWNGRADING SCHEDULE

16. DISTRIBUTION STATEMENT *(of this Report)*

Approved for public release; distribution unlimited.

17. DISTRIBUTION STATEMENT *(of the abstract entered in Block 20, if different from Report)*

18. SUPPLEMENTARY NOTES

19. KEY WORDS *(Continue on reverse side if necessary and identify by block number)*

Entrainment Rates

Oscillated Jet

20. ABSTRACT *(Continue on reverse side if necessary and identify by block number)*

A study was made of the nozzle efficiency and

entrainment rates of jets which were made to oscillate by

fluidic means. The entrainment rates were determined using

conventional pitot-static tubes which indicated significant

DD ,FORM 1473 EDITION OF 1 NOV 65 IS OBSOLETE
1 JAN 73
(Page 1)   S/N 0102-014-6601 |

(20. ABSTRACT Continued)

increases for the oscillatory jet versus the steady jet. Also, work was started to verify these results using the Ricou-Spalding entrainment chamber.

2

An Experimental Investigation
of the Efficiency and Entrainment Rates
of a Fluidically Oscillated Jet

by

Richard James Veltman
Lieutenant, United States Navy
B.S., United States Naval Academy, 1969

Submitted in partial fulfillment of the
requirements for the degree of

MASTER OF SCIENCE IN AERONAUTICAL ENGINEERING

from the

NAVAL POSTGRADUATE SCHOOL
June   1976

ABSTRACT

A study was made of the nozzle efficiency and entrainment
rates of jets which were made to oscillate by fluidic means.
The entrainment rates were determined using conventional
pitot-static tubes which indicated significant increases
for the oscillatory jet versus the steady jet. Also, work
was started to verify these results using the Ricou-Spalding
entrainment chamber.

TABLE OF CONTENTS

LIST OF TABLES

LIST OF FIGURES

ACKNOWLEDGMENT

I.   INTRODUCTION

A considerable amount of information exists on the aerodynamic characteristics of steady turbulent jets, but little is known about unsteady jets. Oscillating jets have become of increasing interest in a number of applications, such as increasing the entrainment rates in ejectors used for aircraft thrust augmentors. Other possible applications occur in lasers and ram jets.

An ejector is a simple device designed to increase the thrust from a primary nozzle by the entrainment of secondary air from the surroundings. A schematic of an ejector is shown in Figure 1. It provides for the transfer of energy from the high velocity, low mass flow from the nozzle to the low velocity, high mass flow from the surroundings. The momentum leaving the ejector is greater than that of the primary nozzle alone, and hence the thrust is increased.

Viets [Ref. 2] suggested oscillation of the jets by acoustic techniques in order to increase their mixing and entrainment rates. A design based on his suggestion is shown in Figure 2.

The design allows for a throat area and a larger exit area, separated by a slot. The flow leaving the throat is bistable and will attach to one wall or the other in the exit area. A low pressure area is set up in the slot on the attachment side, while a high pressure forms in the

10

opposite slot. From these pressure areas, pressure waves travel through a tube connecting the slots. The high pressure wave travels to the side of attachment and forces the flow to detach. At the same time, the low pressure wave travels to the opposite slot and draws the flow toward it. Once the flow has attached to the opposite wall, the process is repeated.

Schum made a study [Ref. 1] of several nozzle configurations, steady and unsteady, which might have merit for application in aircraft augmentors. Besides the design suggested by Viets, he also investigated the "flip-flop" and "hypermixing" nozzles, among others. Further information about these designs can be found in Refs. 1 and 2. In his study he showed that the thrust augmentation is proportional to the product of the primary nozzle efficiency and the square root of the entrainment. Therefore an optimum design would be one with a high entrainment rate and high efficiency. Schum's investigation indicated that oscillating jets had the potential to meet these criteria.

The objective of this work was to study the efficiency and entrainment rates of Viets' nozzle in order to provide further information about unsteady jets and thus to contribute to the assessment of their usefulness in aircraft augmenter applications. The tests were conducted using a conventional pitot-statis tube, with some preliminary work begun using an entrainment chamber similar to that described

in Ref. 5. Typical Reynolds numbers were on the order of 10^5, based on the smaller nozzle dimension.

II. THRUST AND EFFICIENCY

Air was exhausted from a plenum chamber into the atmosphere through a row of nozzles separated from each other by sheets of one-eighth inch aluminum. The plenum was supplied with air which was run from a holding tank through a pressure regulator. A mercury "U" tube was used to read the gage pressure in the plenum chamber.

The chamber was mounted on a frame, but was free to slide forward and backward in the direction of the thrust. A bar and thrust ring was attached to the upwind side of the plenum and to the frame, with a strain gage bonded to the thrust ring. The output of the strain gage was put through an amplifier and wheatstone bridge, and displayed on a digital voltmeter. Figures (3) and (4) show the experimental setup.

All of the tests were conducted using a constant back pressure (ambient), changing the plenum pressures to vary the pressure ratio.

The efficiency of a nozzle is defined as the ratio of the measured thrust to the ideal (isentropic) thrust. The actual thrust was measured by setting the desired plenum pressure and recording the strain gage output. The strain gage had been calibrated by suspending a tray from the upwind side of the plenum, adding known weights, and recording the strain gage output. By plotting the output versus the

13

weight, a calibration curve had been obtained. The actual
thrust was then a simple conversion of millivolts to pounds
force by using the curve.

By oscillating the flow, a portion of the momentum
leaving the nozzle is in the transverse direction. This
necessarily decreases the streamwise component for a given
flow rate. For this reason, reduced efficiencies were
expected.

The theoretical thrust is given by the momentum equation.

$$F_{net} = \underset{out}{\int} \rho v (v \cdot dA) - \underset{in}{\int} \rho v (v \cdot dA) \tag{1}$$

Assuming one-dimensional flow, and assuming the $V_{in} = 0$
due to a large reservoir area compared with the nozzle
area,

$$F_{net} = \rho v^2 A = P A \gamma M^2 \tag{2}$$

For isentropic flow,

$$P_O = P [1 + \frac{\gamma-1}{2} M^2]^{-\frac{\gamma}{\gamma-1}} \tag{3}$$

which can be arranged to express M^2 in terms of the
pressure ratio.

$$M^2 = [(\frac{P}{P_O})^{\frac{1-\gamma}{\gamma}} - 1] \frac{2}{\gamma-1} \tag{4}$$

14

Substituting for M^2, the momentum equation becomes

$$F_{net} = PA\left(\frac{2\gamma}{\gamma-1}\right)\left[\left(\frac{P}{P_o}\right)^{\frac{1-\gamma}{\gamma}} - 1\right]$$ (5)

or in dimensionless form,

$$\frac{F}{P_o A} = \frac{P}{P_o}\left(\frac{2\gamma}{\gamma-1}\right)\left[\left(\frac{P}{P_o}\right)^{\frac{1-\gamma}{\gamma}} - 1\right]$$ (6)

The critical pressure ratio for choked flow in the nozzle can be determined from equation (3), using $M = 1$ and $\gamma = 1.4$.

$$P_o = P\left[1 + \frac{1.4-1}{2}(1)^2\right]^{\frac{-1.4}{.4}}$$

$$\left(\frac{P}{P_o}\right)_{critical} = .5283$$

For flows with P/P_o less than $(P/P_o)_{critical}$, the exit of a converging nozzle is choked and $M = 1$ is the maximum Mach number attainable. With constant back pressure, the plenum pressure can be increased to decrease P/P_o below the critical value. For these conditions, there is an additional force: $F = (.5283P_o - P)A$. Therefore, the thrust equation becomes

$$\frac{F}{P_o A} = \frac{P}{P_o}\left(\frac{2\gamma}{\gamma-1}\right)\left[\left(\frac{P}{P_o}\right)^{\frac{1-\gamma}{\gamma}} - 1\right]$$ (7)

or

$$\frac{F}{P_O A} = \frac{P}{P_O}(\frac{2\gamma}{\gamma-1})\,[\,(\frac{P}{P_O})^{\frac{1-\gamma}{\gamma}} - 1] + (.5283P_O - P)A \quad (8)$$

for pressure ratios below critical.

Another approach to the non-dimensional thrust equation is

$$F = \frac{w}{g}\, a\, M$$

$$F = \frac{w}{g}\,\sqrt{\gamma R}\quad \frac{T}{T_O}\,\sqrt{T_O}\, M$$

$$\frac{F}{w\sqrt{T_O}} = \frac{\sqrt{\gamma R}}{g}\, M\quad \frac{T}{T_O}$$

For isentropic flows, the temperature ratio can be expressed in terms of the pressure ratio. Substituting, the thrust equation becomes

$$\frac{F}{w\sqrt{T_O}} = \frac{\sqrt{\gamma R}}{g}(\frac{P}{P_O})^{-\frac{\gamma-1}{2\gamma}}\{[(\frac{P}{P_O})^{\frac{1-\gamma}{\gamma}} - 1]\frac{2}{\gamma-1}\}^{\frac{1}{2}}$$

or

$$\frac{F}{w\sqrt{T_O}} = \frac{\sqrt{\gamma R}}{g}(\frac{P}{P_O})^{-\frac{\gamma-1}{2\gamma}}\{[(\frac{P}{P_O})^{\frac{1-\gamma}{\gamma}} - 1]\frac{2}{\gamma-1}\}^{\frac{1}{2}} + (.5283P_O - P)A$$

for supercritical pressure ratios.

The ideal thrust was computed using equation (5), assuming a plain converging nozzle. The area was measured to be 2.492 in^2 for five nozzles operating, and 1.484 in^2 when only three nozzles were utilized.

The efficiencies obtained were lower than expected, possibly due to flow separation at the outer walls. In an effort to correct this, the outer two nozzles were blocked off, and the tests were run again using only the three inner nozzles. The resulting efficiencies were lower than those for all five nozzles operating.

To improve the performance, a new inlet was designed to provide for a more gradual reduction of area from the plenum to the nozzles. The apparatus was recalibrated, yielding approximately the same curve.

With the new inlet, the efficiencies were basically unchanged at lower plenum pressures, but were slightly higher at pressures above 20 inches of mercury gage. Again the two outer nozzles were blocked off, but the efficiencies remained at about the same level.

III.   FREQUENCY OF OSCILLATION

The primary method used to determine the frequency of oscillation was to connect a pitot tube to a pressure transducer, and feed the output of the transducer to a spectral analyser. The desired plenum pressure was set, and the pitot tube was inserted in the flow in the center of the nozzle exit. By placing the pitot tube in that location, the pressure transducer sensed the flow twice for each cycle. That is, if the flow started at the upper wall, detached, and reattached to the lower wall, it passed the pitot tube and was felt by the transducer. To complete one full cycle, the flow would detach from the lower wall and reattach to the upper wall, again passing the pitot tube. For this reason, the frequencies listed in Tables 4 through 9 are actually twice the frequency of oscillation.

The first frequency measurements were taken with all five nozzles operating. The data in Table 4 show that for all plenum pressures used, the two outer nozzles were consistently lower in frequency than the inner three. The two outer nozzles were then blocked off, and frequency measurements taken for the three inner nozzles, and the data listed in Table 5. A comparison of Tables 4 and 5 shows that no major change in observed frequency occurred. For this reason, it was felt appropriate to keep the outer nozzles blocked off for all further tests.

To remain consistent in the presentation of the data, the nozzles were numbered, and this numbering system retained throughout the tests. Therefore, the column headings in some of the data tables and the explanatory information in the figures indicate nozzles 2, 3, or 4. Nozzles 1 and 5 were the outer nozzles which were blocked off.

After taking another set of measurements to insure consistency and repeatability, the length of the feedback tubes was changed, and frequencies measured. The tube length for each set of measurements is given below the appropriate table.

An alternative method used to determine the frequency was to connect a microphone to the analyser and pass the microphone in the vicinity of the flow. This method was used to corroborate the data taken with the transducer. For these measurements, the tube length was 6 feet, and a comparison between tables 7 and 10 shows close agreement. At higher plenum pressures, an input power warning light was illuminated on the analyser, necessitating removal of the microphone to a greater transverse distance from the flow field. At this greater distance, approximately 8 inches from the exit centerline, the microphone was unable to distinguish any frequency difference between the individual nozzles, as can be seen in Table 10.

Viets, in Ref. 2, provided two plots of frequency, one as a function of stagnation pressure and the other as a

19

function of feedback tube length, for nozzles of similar
design that he had investigated.   These have been reproduced
as Figures 9 and 10 for comparison purposes.   The data
obtained during this study are presented in Figure 11.

IV.   VELOCITY PROFILES

Velocity profiles were taken utilizing a pitot static tube connected to a manometer. Two axial distances were used, three and nine inches from the exit. With the tube set at an axial location, it was then moved in the transverse direction and manometer readings recorded. A mercury manometer was used at three inches from the exit while Dyer fluid (specific gravity = 1.75) was used at nine inches. For convenience, all manometer readings have been converted to inches of mercury.

Profiles were taken for the three inner nozzles operating in the oscillating and non-oscillating modes. The latter was accomplished by disconnecting the feedback tubes, leaving the slots open to the atmosphere. All profiles were taken using a plenum pressure of 10 inches of mercury gage. The raw data are presented in Tables 11 through 22.

An available computer subroutine was used to generate additional data points by interpolating between given points using standard numerical techniques. A total of 161 points were then used in another subroutine to provide a smooth curve on a Calcomp plotter. These dimensional profiles are given in Figures 12 through 23.

Non-dimensional velocity profiles were plotted to compare the flow at both axial stations for the individual nozzles in the steady and oscillating modes. These profiles are

given as Figures 24 through 29. In the non-oscillating mode, all three nozzles show good agreement with two-dimensional turbulent jet theory [Ref. 3]. While it is inappropriate to compare this theory with the oscillating flow, the profiles of the oscillating nozzles do indicate that the flow patterns are basically similar at both stations.

It should be pointed out that the method used in these tests provides only an average velocity in the case of oscillating flow, because at any point in the flow field the velocity will vary from zero to some maximum value, depending on the location of the flow at that instant. An independent study [Ref. 4], to be published, conducted velocity profile surveys of a similar nozzle using laser velocimetry and a pitot-static tube. Integration of these profiles indicated that the entrainment rates obtained by the pitot-static tube were approximately 10 per cent higher than those using laser velocimetry techniques.

V. ENTRAINMENT

A qualitative comparison of the entrainment rates of a
nozzle in the steady and oscillating modes was made by
integrating the velocity profiles using a planimeter. The
information obtained is presented in Table 23, along with
the percentage increase in area of the oscillating over the
steady case for each nozzle at the specified axial location.
Due to inaccuracies in the pitot-static tube velocity pro-
files, a more exact and direct method was desired to measure
the entrainment rates.

Reference 5 describes a method for measuring the axial
mass flow rate of a turbulent jet with the secondary flow
it entrains. This technique consisted of metering flow to
a primary jet which was injected into a porous-walled
cylindrical chamber, and metering secondary flow which was
injected through the porous walls of the chamber. The base
of the chamber was closed except for an aperture from which
the primary jet was injected, while the upper end of the
cylinder was partially closed off by an exit orifice. The
secondary flow was adjusted until the axial pressure gradi-
ent across the exit orifice went to zero, when it was assumed
that the "entrainment appetite" of the jet was satisfied.

In Ref. 6, Weiss describes a chamber patterned after
that of Ricou and Spalding, with one basic difference. In
Ricou's and Spalding's chamber, the axial location of the

exit and hence the length of the entrainment chamber was fixed, but the orifice diameter could be changed. In Weiss' chamber, see Figure 30, the exit orifice was incorporated into the base of a concentric cylinder, with non-porous walls, which was free to slide up and down within the porous-walled cylinder. The concentric cylinder was designed for a tight fit with the porous-walled cylinder, such that secondary air could leave the chamber only through the entrainment process. With this design the axial location of the exit orifice became variable. Hence, while the work described in ref. 5 was directed toward finding an optimum exit orifice diameter, the work in ref. 6 was directed toward finding an optimum axial distance for a given orifice diameter.

The entrainment studies conducted in this work utilized Weiss' equipment. However, due to physical limitations of the apparatus as modified to fit a fluidically oscillated nozzle, it was not possible to meter the flow to the primary jet. For this reason, the plenum pressure was always set at 4 inches of mercury gage. This insured that the same primary mass flow rate was used for all the tests, thereby avoiding the metering problem. The secondary flow was metered by a venturi.

The procedure used in the tests was as follows. A micromanometer, which was used to measure the axial pressure gradient across the exit orifice, was zeroed by bringing the

24

fluid level to a crosshair, and the reading recorded. The plenum pressure and secondary flow were set, and the microm-anometer was adjusted to bring the fluid level back to the crosshair. This reading and the pressure drop across the venturi were then recorded. The secondary flow was then increased or decreased as desired, and the new readings were recorded.

The data for the initial runs, as presented in Tables 24 through 30, were taken using a mercury "U" tube to measure the pressure drop across the venturi. The mass flow rate, as discussed in ref. 6, is proportional to the square root of this pressure drop. Due to the uncertainty in the second decimal place of the reading, estimated at ± .03 inches, these data were considered adequate only in the context of determining the optimum axial distance for the orifice. Figure 31 is a plot of the square root of the pressure drop, for zero pressure gradient across the orifice, versus the axial distance. It clearly shows a peak entrainment at about 4.5 inches.

After determining this optimum distance, a manometer containing fluid with specific gravity of 1.75 was substi-tuted for the "U" tube, and additional tests were run with the orifice at axial locations in the vicinity of 4.5 inches. Tables 31 through 33 present these data.

An initial plot of these data indicated that more data points were required at the axis crossover point, i.e.,

near the point where the chamber pressure was atmospheric. These points had a different zero reading on the microm-anometer than any of the others, and therefore are listed separately in Tables 34 through 36.

The data listed in Tables 31 through 36 are plotted in Figure 32.

VI. CONCLUSIONS AND RECOMMENDATIONS

The efficiencies measured in this work are within the range of those measured by Viets [Ref. 7] for similar nozzles. Unfortunately, attempts to increase the efficiencies were not completely successful.

A preliminary number of velocity profiles were obtained using a pitot-static tube. A profile was taken for each nozzle at two separate distances downstream for the oscillating and steady cases. The accuracy of these profiles is in doubt for the oscillating case, as previously explained. However, Ref. 4 shows that the error is not likely to exceed 12 to 15 per cent. Therefore, the results of this study seem to indicate that the fluidically oscillated jet has significantly higher entrainment rates than steady jets. It is interesting to note that the velocity profile for nozzle number 3 shows the most pronounced "double hump" profile, which is characteristic of oscillated flows. At the same time, Table 23 shows that nozzle number 3 had the most significant increase in entrainment.

Some preliminary work was done using an entrainment chamber, but time was insufficient to investigate the entrainment rates of the oscillating jet to compare with the steady jet. Therefore, it is not possible at this time to provide more accurate entrainment information than that presented in Table 23.

A more detailed velocity profile survey is recommended. More vertical planes should be used to provide a more accurate picture of the overall flow field. In addition, the outer nozzles should be unblocked to determine what effect, if any, their operation has on the profiles of the inner nozzles. As obtained in this study, the oscillating profile does not change significantly from the steady profile for nozzles 2 and 4. This may not be the case when nozzles 1 and 5 are operating.

Further development of the entrainment chamber is required for a thorough study of the entrainment rates of the oscillating jets. At present, insufficient secondary air is available, which limits the plenum pressures that can be used. It is therefore recommended that additional lines be incorporated to supply secondary air to the chamber.
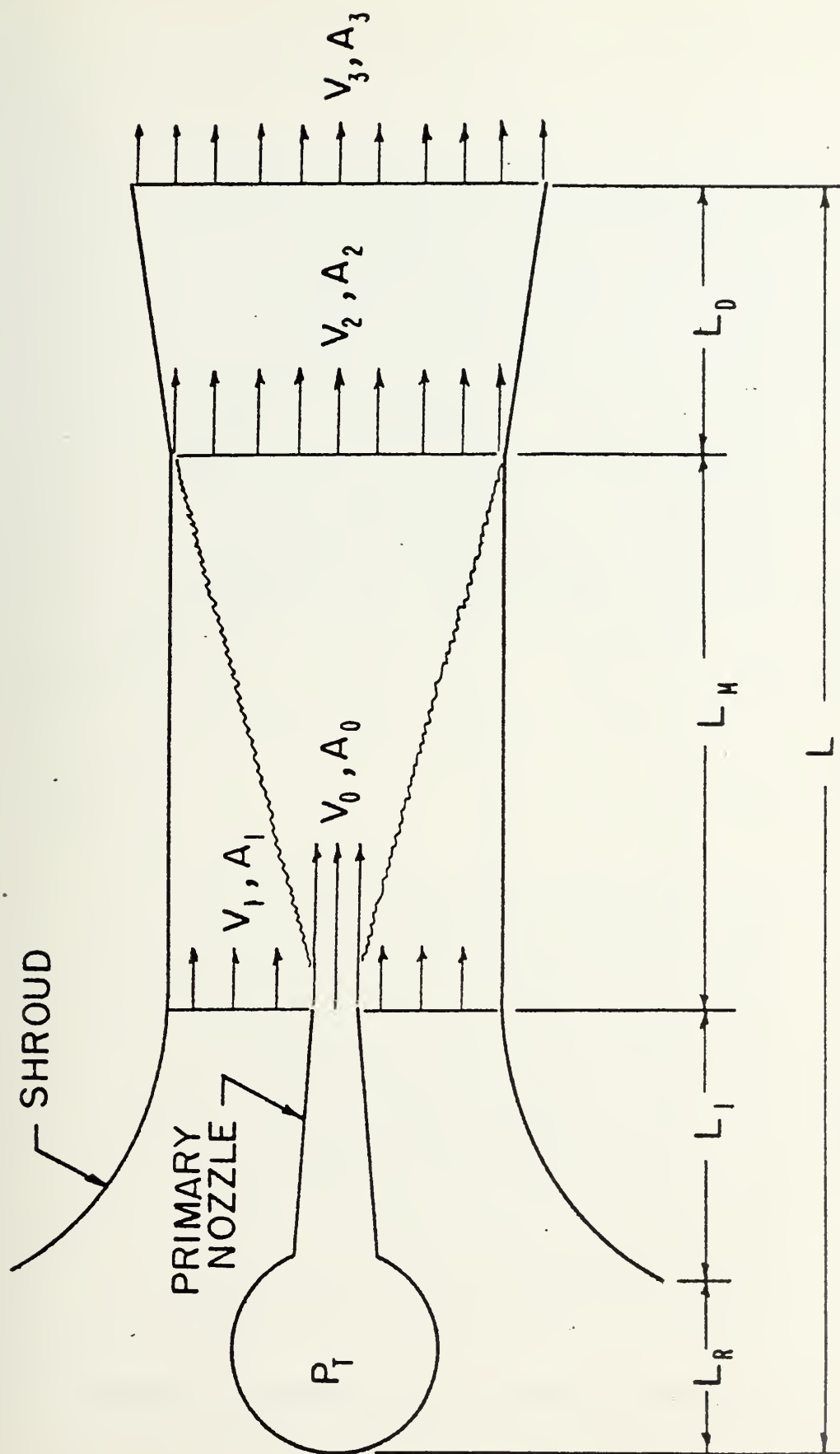
Figure 1. The ejector principle[1]
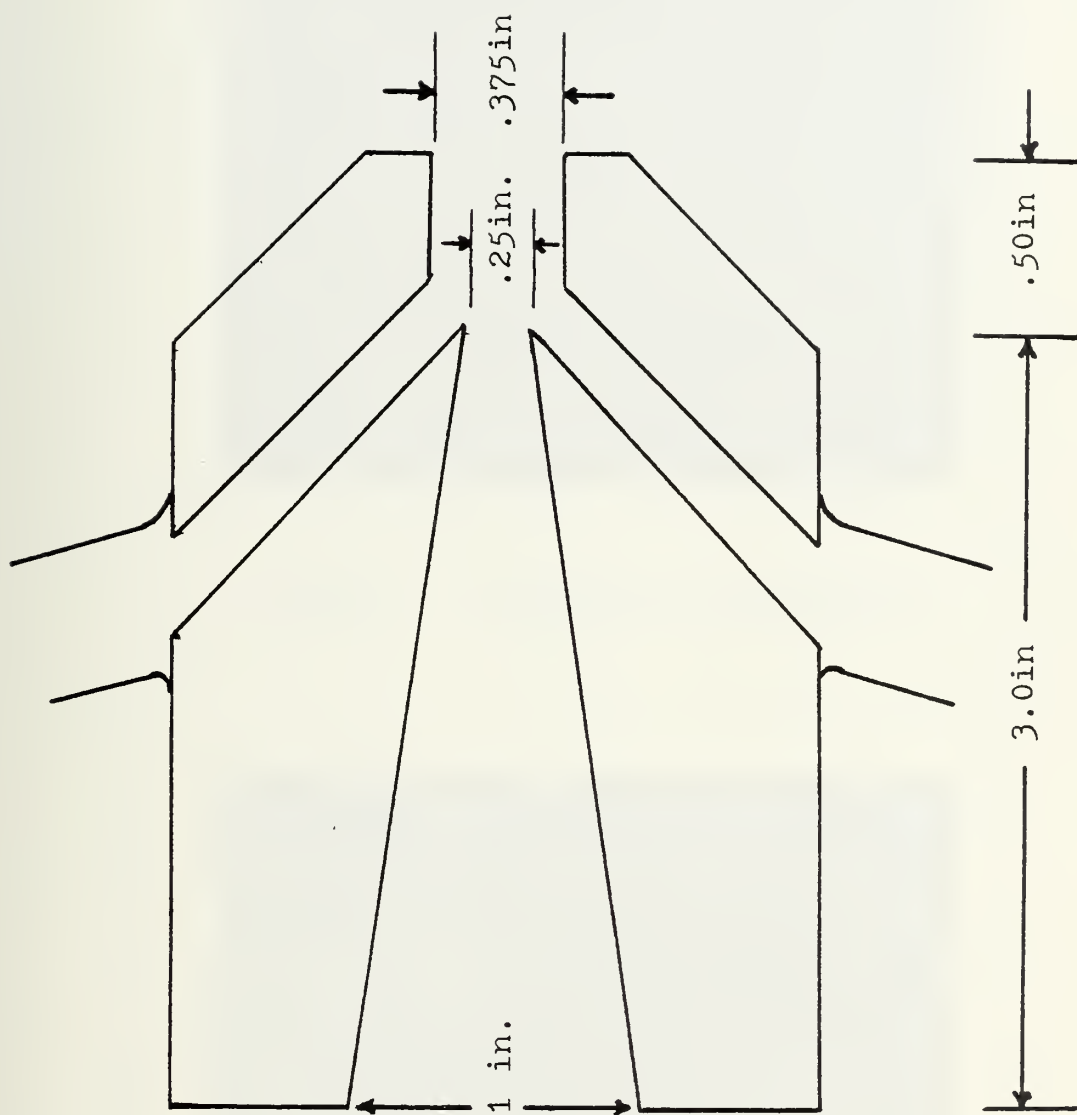
Figure 2. Schematic of fluidically oscillated nozzle
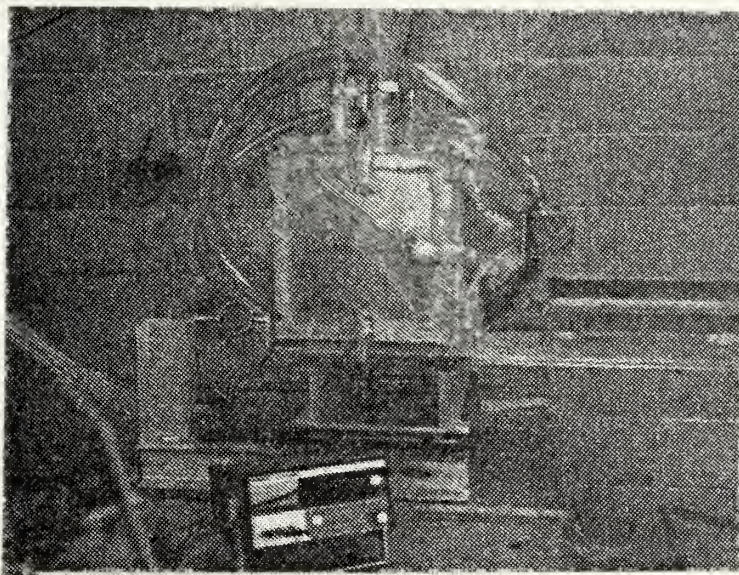
Figure 3. Experimental Apparatus
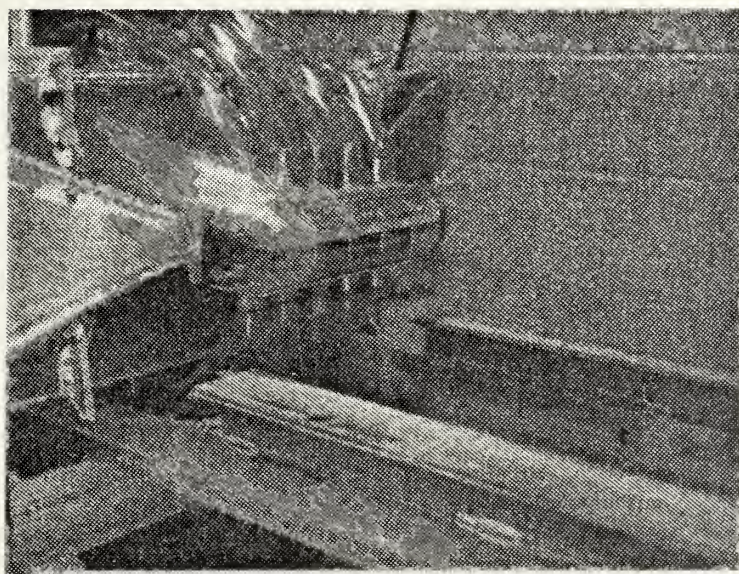
Figure 4. Nozzle Configuration used in Tests
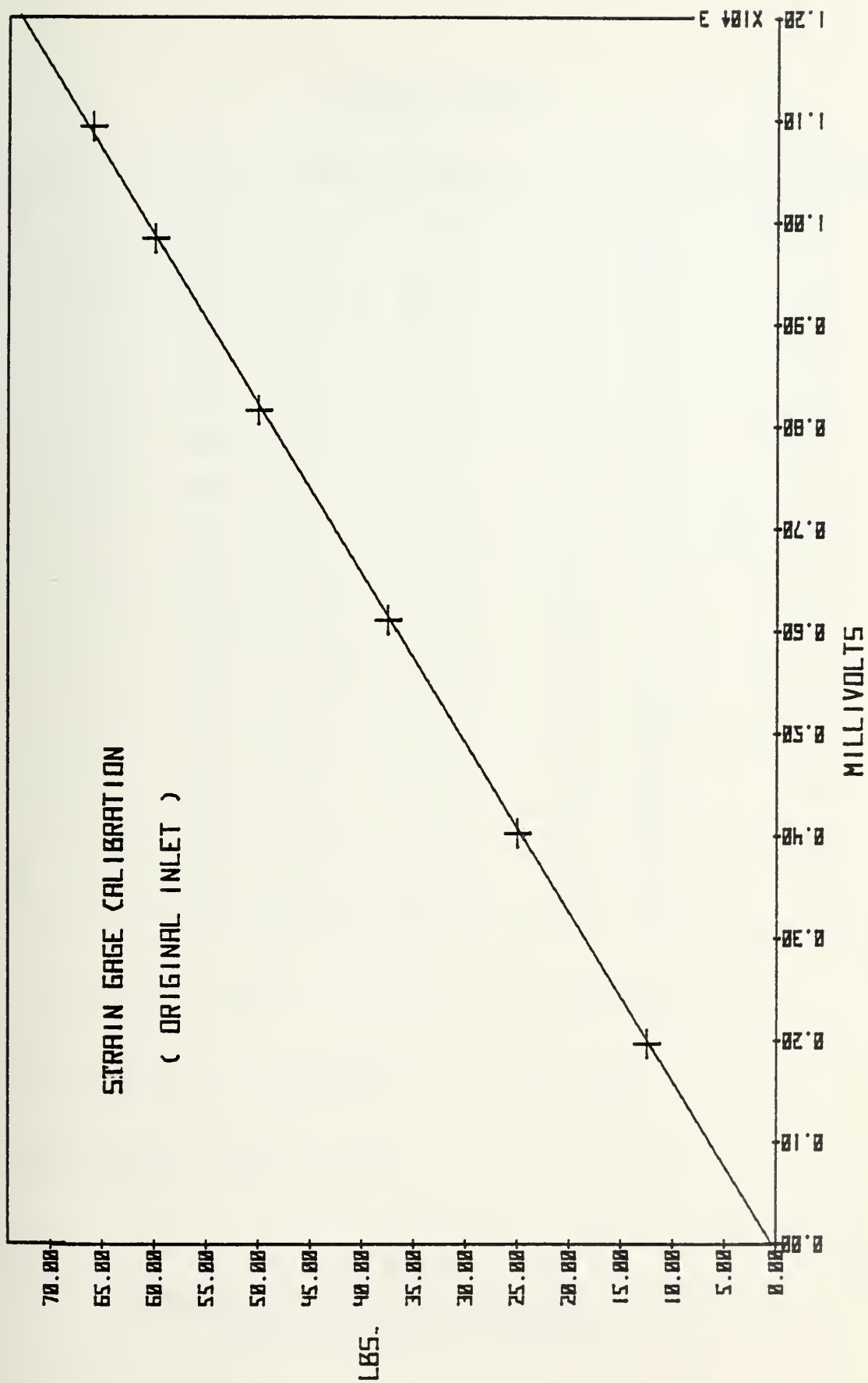
Figure 5. Strain gage calibration curve for original inlet

ORIGINAL INLET

P_G	mV	P/P_o	F_{act}	F_{ideal}	η	$(\frac{F}{P_o A})_{act}$	$(\frac{F}{P_o A})_{ideal}$
8	242	.789	14.72	17.99	.82	.317	.387
9	276	.769	16.79	20.01	.84	.352	.420
10	306	.749	18.61	22.10	.84	.380	.450
11	331	.731	20.13	24.05	.84	.401	.479
12	356	.714	21.66	25.94	.83	.422	.505
13	380	.697	23.12	27.90	.83	.440	.530
14	405	.681	24.64	29.79	.83	.458	.552
15	426	.666	25.91	31.62	.82	.471	.574
16	456	.652	27.74	33.38	.83	.493	.593
17	477	.638	29.02	35.18	.82	.505	.612
18	502	.624	30.54	37.04	.82	.520	.629
19	527	.612	32.06	38.67	.83	.535	.645
20	551	.599	33.52	40.49	.83	.548	.660
21	577	.588	35.10	42.07	.83	.563	.674
22	597	.576	36.32	43.83	.83	.571	.687
23	615	.565	37.41	45.49	.82	.577	.700
24	642	.555	39.05	47.04	.83	.591	.712
25	664	.545	40.39	48.62	.83	.600	.722
26	690	.535	41.97	50.24	.84	.613	.733

$P_a = 29.96$ in. Hg. $\qquad$ $P_G =$ in. Hg

$A = 2.492$ in^2 (5 nozzles) $\qquad$ $F =$ lbs.

Tube length: 6 Ft. 4 In.

TABLE I

Thrust and efficiency data for original
inlet utilizing 5 nozzles

33

ORIGINAL INLET

P_G	mV	F_{act}	F_{ideal}	η
5	85	5.17	6.88	.75
6	104	6.33	8.18	.77
7	120	7.30	9.47	.77
8	137	8.33	10.69	.78
9	154	9.37	11.89	.79
10	170	10.34	13.13	.79
11	183	11.13	14.29	.78
12	200	12.17	15.41	.79
13	214	13.07	16.57	.79
14	227	13.81	17.70	.78
15	243	14.78	18.79	.79
16	258	15.69	19.91	.79
17	273	16.61	20.90	.79
18	287	17.46	22.01	.79
19	287	18.49	23.06	.80
20	320	19.47	24.06	.81
21	335	20.38	25.08	.81
22	346	21.05	26.04	.81
23	362	22.02	27.03	.81
24	373	22.69	27.95	.81
25	387	23.54	28.89	.81

P_a = 29.90 in. Hg P_G = in. Hg

A = 1.484 in^2 (3 nozzles) F = lbs

Tube length: 6 Ft. 4 In.

TABLE II
Thrust and efficiency data for original inlet

34
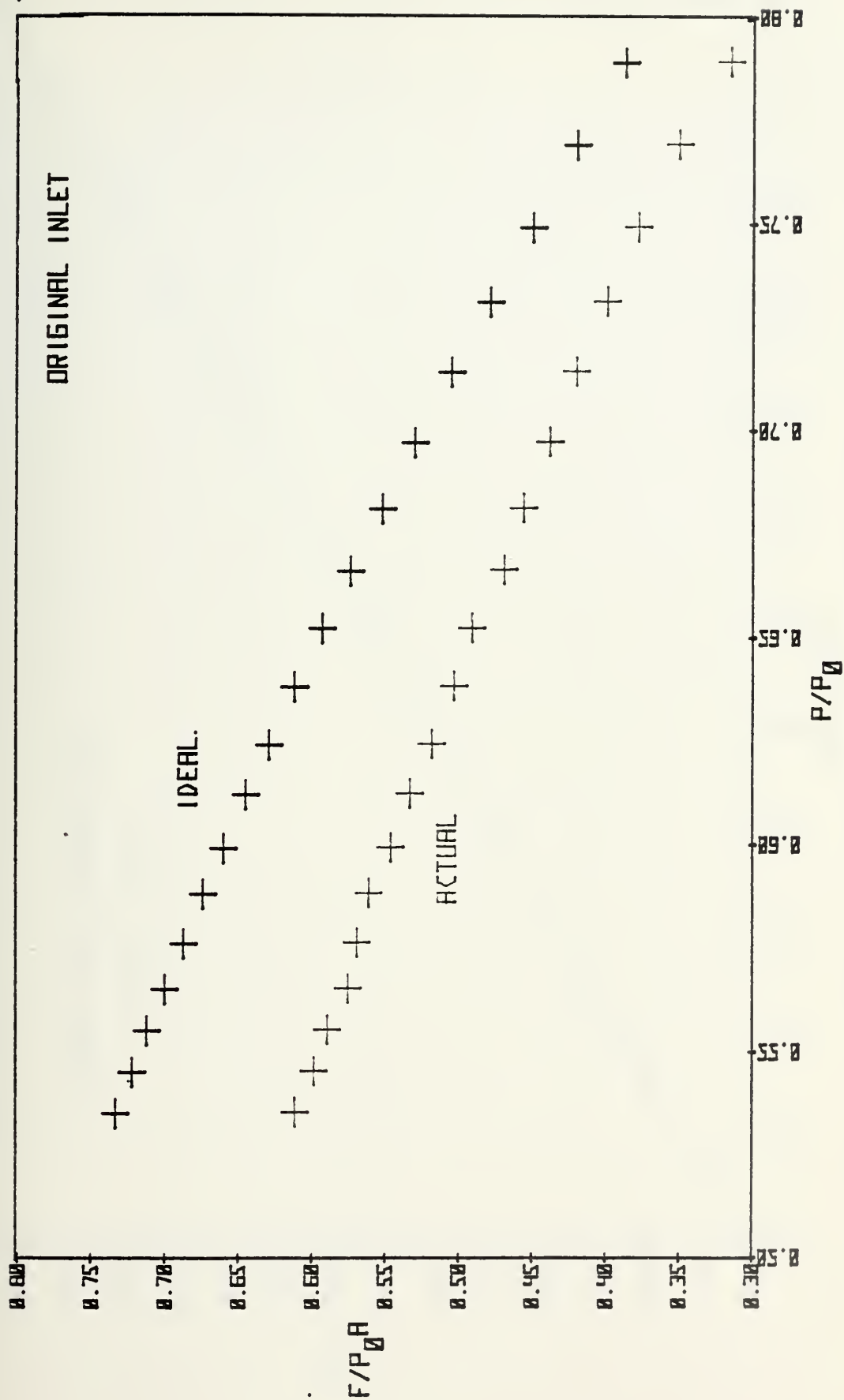
Figure 6. Non-dimensional thrust vs pressure ratio for original inlet
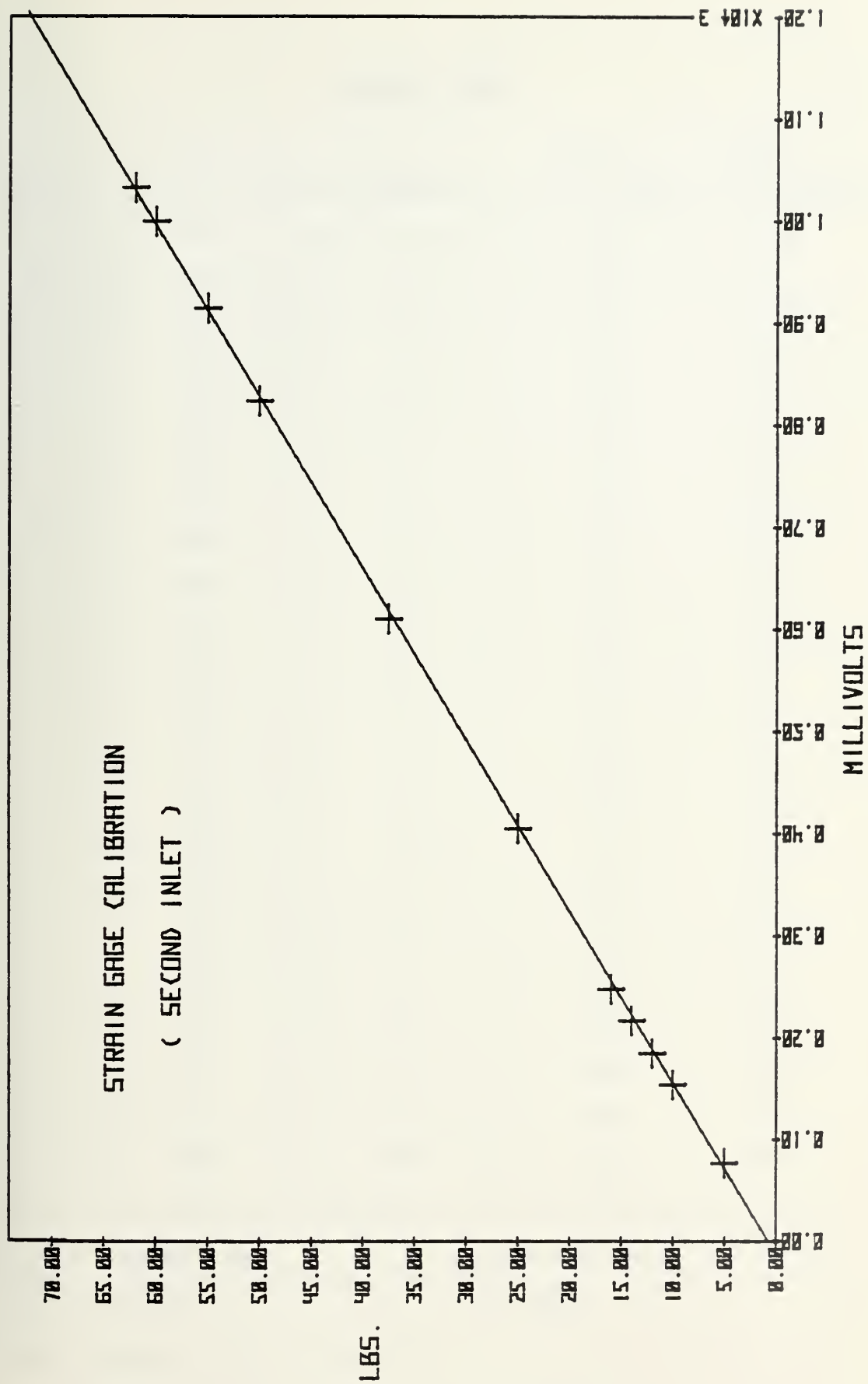
Figure 7. Strain gage calibration curve for second inlet

P_G	mV	$\frac{P}{P_o}$	F_{act}	F_{ideal}	η	$(\frac{F}{P_o A})_{act}$	$(\frac{F}{P_o A})_{ideal}$
5	157	.857	9.55	11.62	.82	.222	.270
6	184	.834	11.19	13.72	.82	.253	.311
7	214	.811	13.02	15.90	.82	.287	.350
8	247	.790	15.02	17.96	.84	.322	.385
9	275	.770	16.73	19.98	.84	.350	.418
10	303	.750	18.43	22.08	.83	.376	.450
11	328	.732	19.95	24.03	.83	.397	.478
12	357	.715	21.72	25.93	.84	.422	.503
13	380	.698	23.11	27.88	.83	.438	.529
14	402	.682	24.45	29.78	.82	.453	.552
15	422	.667	25.67	31.61	.81	.465	.573
16	453	.653	27.55	33.37	.83	.488	.592
17	483	.639	29.38	35.18	.84	.510	.611
18	506	.626	30.78	36.91	.83	.523	.627
19	537	.613	32.66	38.68	.84	.544	.644
20	559	.601	34.00	40.36	.84	.555	.659
21	589	.589	35.83	42.08	.85	.573	.673
22	607	.578	36.92	43.70	.84	.579	.686
23	633	.567	38.50	45.36	.85	.593	.699
24	656	.556	39.90	47.06	.85	.603	.711
25	680	.546	41.36	48.64	.85	.613	.721
26	706	.536	42.94	50.27	.85	.626	.732
27	726	.527	44.16	51.76	.85	.632	.741
28	752	.518	45.74	53.29	.86	.643	.750
29	769	.509	46.78	54.85	.85	.647	.758
30	784	.501	47.69	56.27	.85	.649	.766

P_a = 30.08 in. Hg. P_G = in. Hg.

A = 2.492 in^2 F = lbs

Tube Length: 6 Ft. 4 In.

TABLE III
Thrust and efficiency data for second inlet utilizing
5 nozzles
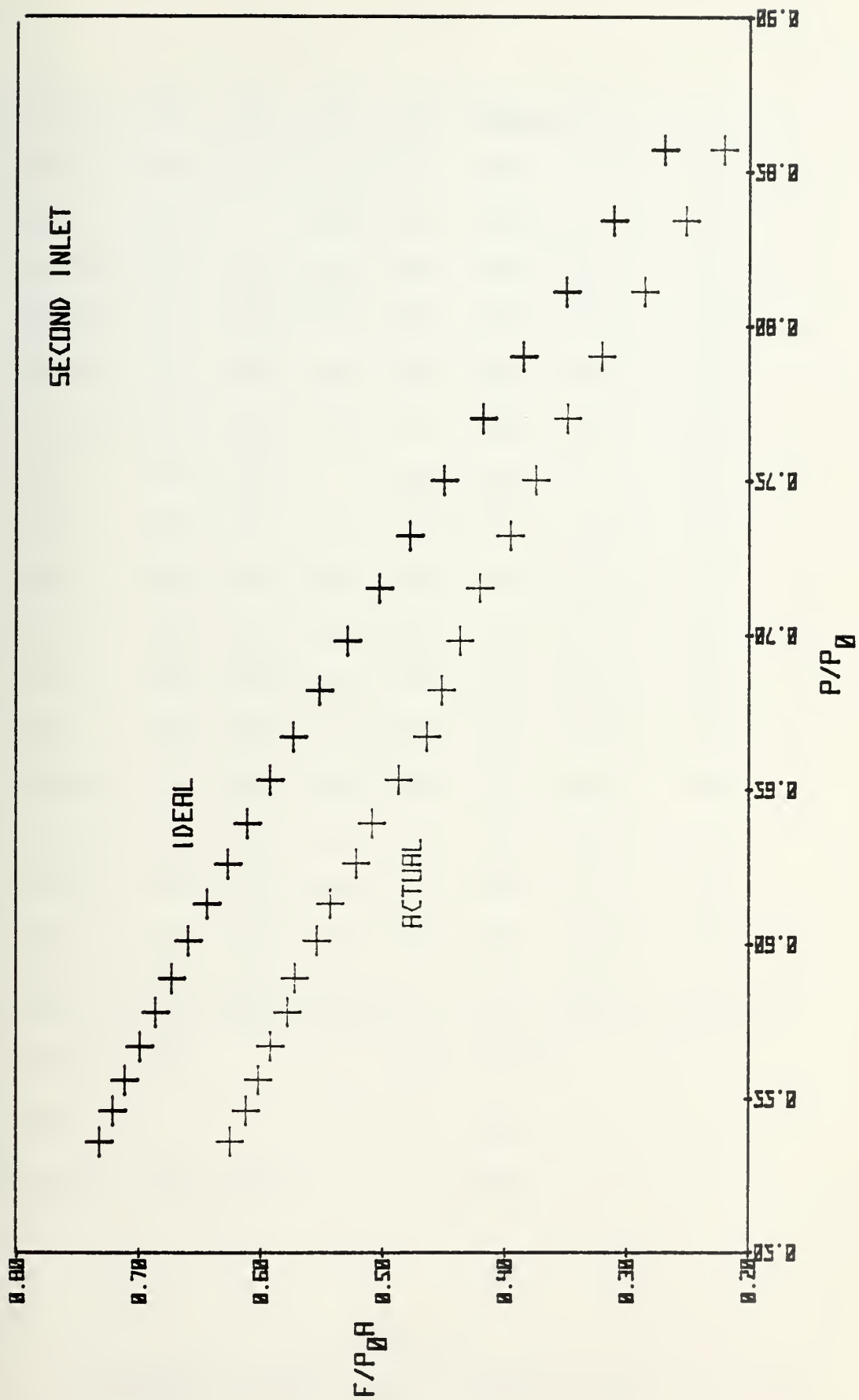
Figure 8. Non-dimensional thrust vs pressure ratio for second inlet

P_G	mV	$f_{\#1}$	$f_{\#2}$	$f_{\#3}$	$f_{\#4}$	$f_{\#5}$	F_{ideal}	F_{act}	η
5	158	82.9	94.1	91.3	93.3	84.1	11.57	9.57	.83
6	191	85.3	94.9	–	95.7	85.3	13.75	11.57	.84
7	221	86.1	95.7	94.5	95.9	85.3	15.87	13.39	.84
8	251	85.7	95.3	92.9	94.5	86.1	17.96	15.20	.85
9	278	86.5	96.1	92.9	94.5	86.5	20.01	16.84	.84
10	305	86.1	96.5	93.3	94.9	86.5	22.02	18.47	.84
11	332	–	96.1	93.3	–	86.5	24.00	20.11	.84
12	356	–	96.9	94.1	–	86.5	25.94	21.56	.83
13	380	–	96.5	94.9	94.9	86.5	27.85	23.02	.83
14	403	–	96.1	94.9	94.9	86.5	29.73	24.41	.82
15	429	–	96.1	95.3	95.3	86.9	31.58	25.98	.82
16	454	–	96.9	95.3	95.3	86.9	33.40	27.50	.82
17	478	86.5	97.3	94.9	96.1	87.7	35.19	28.95	.82
18	509	86.9	96.9	94.9	95.7	87.7	36.95	30.83	.83
19	535	86.9	96.9	95.3	95.3	87.7	38.69	32.40	.84
20	560	86.9	96.1	95.3	95.3	87.7	40.40	33.92	.84
21	587	86.9	96.1	94.9	95.7	87.7	42.09	35.55	.84

P_a = 30.05 in. Hg.　　　　　　P_G = in. Hg.

A = 2.492 in^2　　　　　　　　F = lbs

Tube Length:　5 Ft. 10 In.　　　　f = Hz

TABLE IV

Frequency, thrust, and efficiency data utilizing
5 nozzles, tube length = 5 Ft. 10 In.

39

P_G	mV	$f_{\#2}$	$f_{\#3}$	$f_{\#4}$	F_{ideal}	F_{act}	η
5	91	93.0	91.0	92.6	6.92	5.51	.80
6	113	93.3	-	94.9	8.22	6.84	.83
7	131	94.6	94.1	94.9	9.49	7.93	.84
8	150	94.1	92.6	94.5	10.74	9.09	.85
9	168	95.3	92.9	95.7	11.97	10.18	.85
10	183	-	92.9	94.6	13.17	11.08	.84
11	201	-	93.3	94.9	14.35	12.17	.85
12	215	96.9	94.5	94.5	15.51	13.02	.84
13	230	96.5	94.9	94.9	16.66	13.93	.84
14	245	96.1	94.9	95.7	17.78	14.84	.83
15	259	96.2	95.3	95.7	18.89	15.69	.83
16	274	97.0	94.9	95.7	19.97	16.60	.83
17	286	97.3	94.9	14.9	21.05	17.32	.82
18	302	96.6	94.8	94.6	22.10	18.29	.83
19	317	96.2	94.7	94.7	23.14	19.20	.83
20	334	-	95.0	95.0	24.17	20.23	.84
21	351	95.7	94.5	95.4	25.18	21.26	.84
22	365	95.7	93.3	95.7	26.17	22.11	.84
23	376	-	-	95.7	27.16	22.77	.84
24	390	-	-	95.7	28.13	23.62	.84
25	407	-	95.8	95.4	29.08	24.65	.85

P_a = 30.31 in. Hg. P_G = in. Hg.

A = 1.484 in^2 F = lbs

Tube Length: 5 Ft. 10 In.   f = Hz

TABLE V

Frequency, thrust and efficiency data
Tube length = 5 Ft. 10 In.

40

P_G	mV	$f_{\#2}$	$f_{\#3}$	$f_{\#4}$	F_{ideal}	F_{act}	η
5	91	93.3	91.3	92.9	6.89	5.51	.80
6	110	93.3	-	-	8.19	6.66	.81
7	130	94.5	94.5	94.1	9.46	7.87	.83
8	149	94.1	92.5	94.5	10.70	9.02	.84
9	167	95.3	92.9	94.5	11.92	10.12	.85
10	184	-	93.7	94.9	13.12	11.14	.85
11	199	-	93.3	95.3	14.30	12.05	.84
12	214	96.9	94.5	94.5	15.46	12.96	.84
13	228	96.5	94.9	94.9	16.60	13.81	.83
14	245	96.1	95.3	95.7	17.72	14.84	.84
15	256	-	95.7	95.7	18.82	15.51	.82
16	274	97.7	95.7	96.1	19.90	16.60	.83
17	288	97.3	95.3	95.3	20.97	17.44	.83
18	302	96.5	95.3	95.3	22.02	18.29	.83
19	319	96.9	95.3	95.3	23.06	19.32	.84
20	334	95.3	95.3	95.3	24.08	20.23	.84
21	349	95.7	95.3	95.7	25.09	21.14	.84
22	363	-	94.9	96.1	26.08	21.99	.84
23	376	-	93.3	96.1	27.06	22.77	.84
24	391	-	-	95.7	28.02	23.68	.85
25	405	-	95.7	95.7	28.58	24.53	.85
26	421	-	95.7	95.7	29.92	25.50	.85
27	435	-	95.7	95.7	30.85	26.35	.85
28	451	-	95.7	96.1	31.77	27.32	.86

P_a = 30.21 in. Hg. P_G = in. Hg.

A = 1.484 in^2 F = lbs

Tube Length: 5 Ft. 10 In. f = Hz

TABLE VI
Frequency, thrust and efficiency
data, Tube length = 5 Ft. 10 In.

41

P_G	mV	$f_{\#2}$	$f_{\#3}$	$f_{\#4}$	F_{ideal}	F_{act}	η
3	58	85.8	85.0	85.4	4.23	3.51	.83
4	75	89.0	88.2	88.2	5.57	4.54	.82
5	92	90.7	–	–	6.89	5.57	.81
6	110	90.6	–	91.5	8.19	6.66	.81
7	123	91.0	91.0	91.0	9.45	7.45	.79
8	142	91.4	90.6	90.6	10.70	8.60	.80
9	158	92.2	90.2	90.2	11.92	9.57	.80
10	172	93.3	90.9	90.9	13.12	10.42	.79

P_a = 30.09 in. Hg. P_G = in. Hg

A = 1.484 in^2 F = lbs

Tube Length: 6 Ft. 0 In. f = Hz

TABLE VII

Frequency, thrust and efficiency
data, Tube length = 6 Ft. 0 In.

P_G	mV	$f_{\#2}$	$f_{\#3}$	$f_{\#4}$	F_{ideal}	F_{act}	η
3	59	79.3	77.7	79.3	4.26	3.57	.84
4	75	82.1	80.5	82.1	5.61	4.54	.81
5	95	82.1	82.5	82.9	6.94	5.75	.83
6	112	82.9	-	83.7	8.24	6.78	.82
7	130	83.7	84.1	84.1	9.52	7.87	.83
8	147	83.7	82.9	84.1	10.77	8.90	.83
9	164	84.5	83.3	84.1	12.00	9.93	.83
10	180	84.1	83.3	84.5	13.21	10.90	.83

P_a = 30.30 in. Hg P_G = in. Hg

A = 1.484 in^2 F = lbs

Tube Length: 6 Ft. 6 In. f = Hz

TABLE VIII

Frequency, thrust and efficiency
data, Tube Length = 6 Ft. 6 In.

P_G	mV	$f_{\#2}$	$f_{\#3}$	$f_{\#4}$	F_{ideal}	F_{act}	η
5	94.1	76.5	76.1	76.9	6.90	5.70	.83
6	112	77.3	-	77.3	8.19	6.78	.83
7	129	77.7	77.7	78.1	9.46	7.81	.83
8	148	77.7	76.9	78.1	10.70	8.96	.84
9	166	78.1	76.9	77.7	11.93	10.05	.84
10	182	78.1	77.3	77.7	13.13	11.02	.84
11	197	-	77.3	77.3	14.30	11.93	.83
12	211	78.3	77.3	77.3	15.46	12.78	.83
13	225	78.5	78.1	78.1	16.60	13.63	.82
14	240	78.1	78.1	77.6	17.72	14.54	.82
15	256	78.9	78.5	78.5	18.82	15.51	.82
16	271	79.3	78.5	78.5	19.91	16.41	.82
17	287	78.9	78.1	77.7	20.98	17.38	.83
18	302	78.5	77.7	77.7	22.03	18.29	.83
19	318	78.5	78.1	77.3	23.07	19.26	.83
20	333	78.1	77.7	77.7	24.09	20.17	.84
21	350	78.1	78.3	78.5	25.10	21.20	.84
22	363	78.3	76.1	78.5	26.09	21.99	.84
23	376	78.5	74.5	78.1	27.07	22.77	.84
24	389	-	74.9	78.1	28.04	23.56	.84
25	404	-	75.7	77.7	29.00	24.47	.84

P_a = 30.30 in. Hg P_G = in. Hg

A = 1.484 in^2 F = lbs

Tube Length: 7 Ft. 0 In. f = Hz

TABLE IX

Frequency, thrust and efficiency
data, Tube Length = 7 Ft. 0 In.

P_G	$f_{\#2}$	$f_{\#3}$	$f_{\#4}$
2	80.5	77.8	80.0
3	86.1	84.4	84.6
4	88.6	88.4	89.4
5	89.2	89.3	89.0
6	90.1	90.6	91.0
7	91.0	91.0	91.0
8	90.2	90.2	90.2
9	90.6	90.6	90.6
10	91.0	91.0	91.0
15	93.0	93.0	93.0
20	91.7	91.7	91.7
25	91.4	91.4	91.4

P_a = 30.02 in. Hg. P_G = in. Hg

A = 1.484 in^2 f = Hz

Tube Length: 6 Ft. 0 In.

Frequency data obtained by alternate method.

TABLE X

Frequency data using microphone
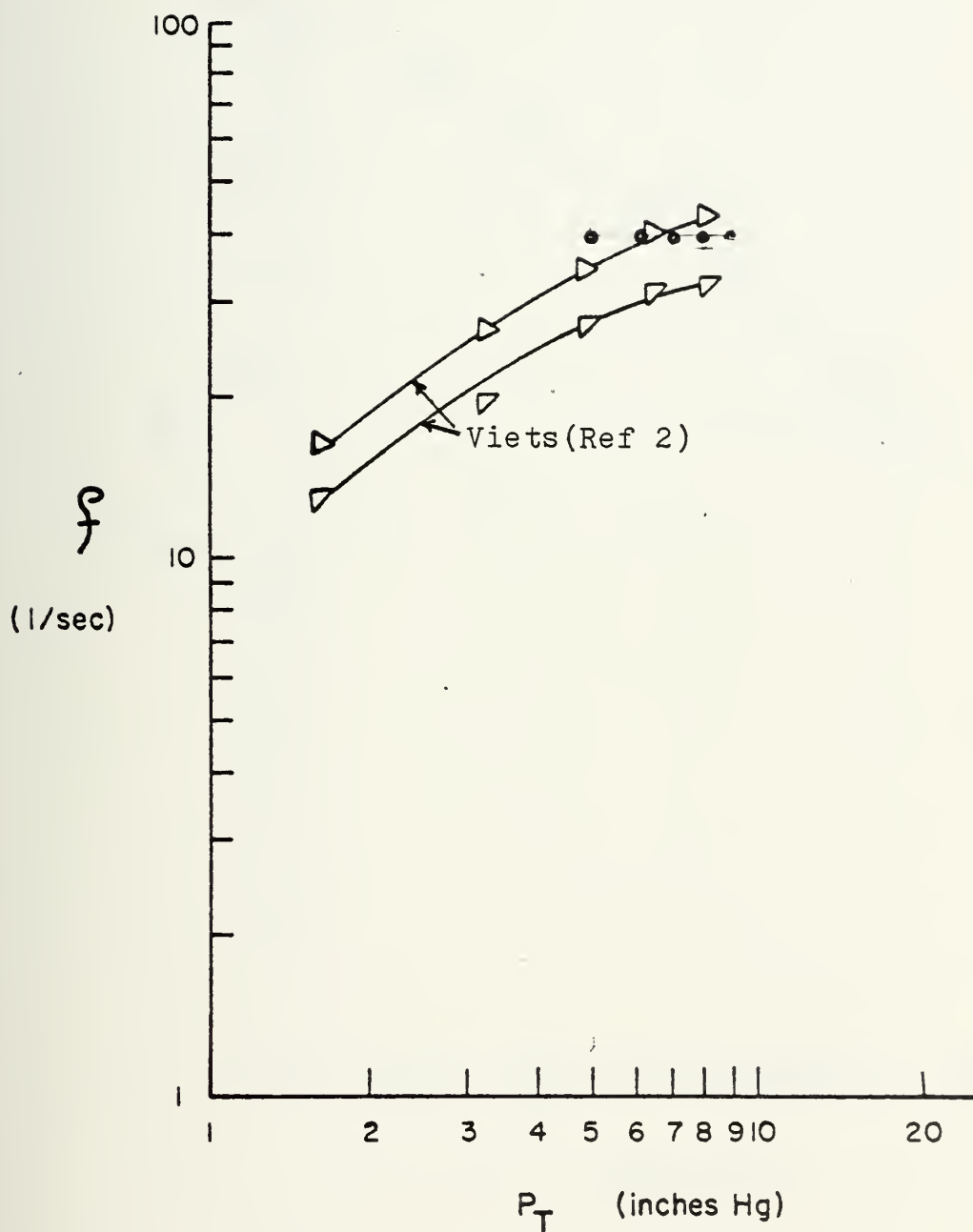method, Tube length = 6 Ft. 0 In.

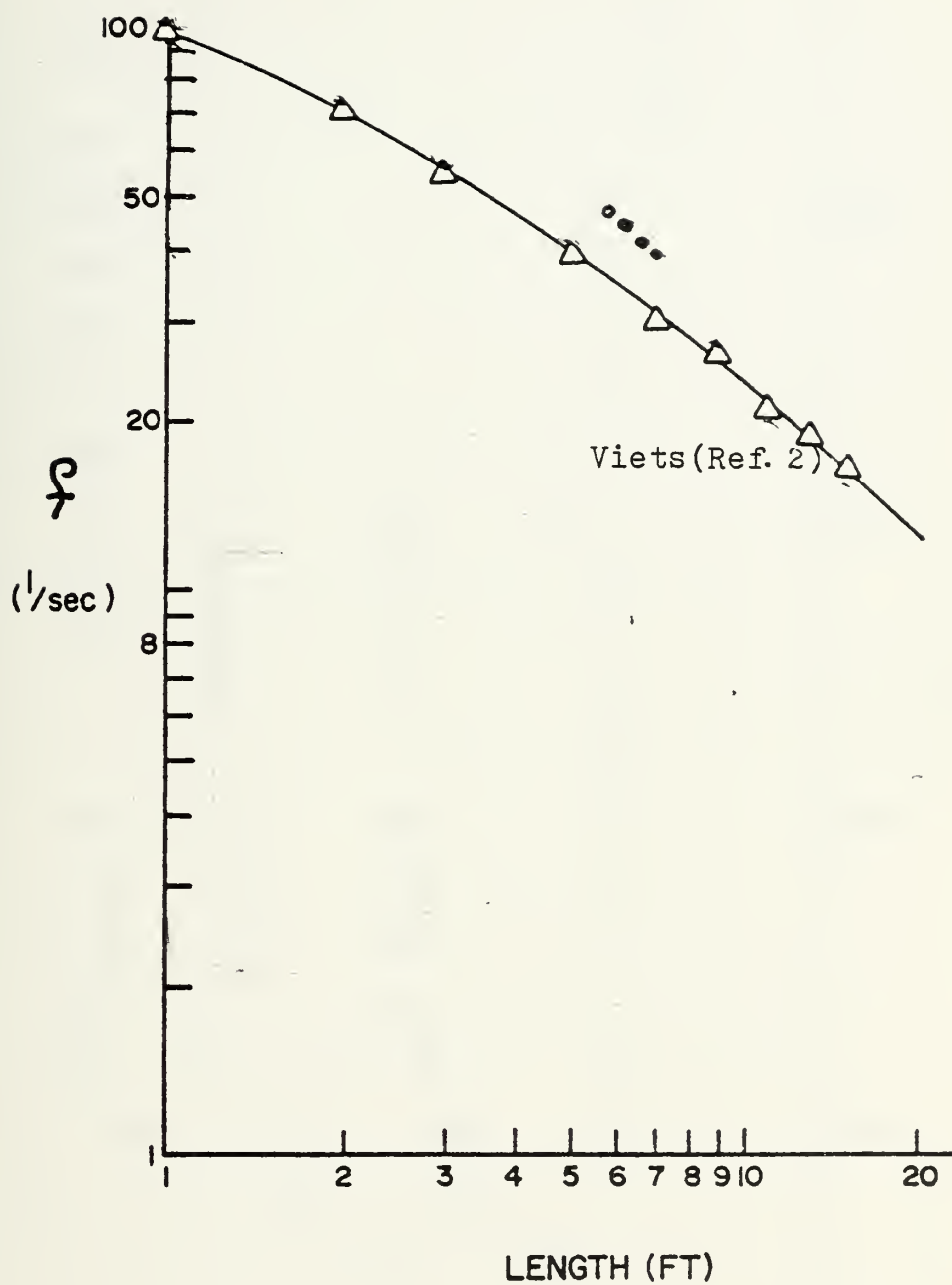Figure 9. Frequency of oscillation vs
            stagnation pressure2

Figure 10. Frequency of oscillation vs
feedback tube length[2]
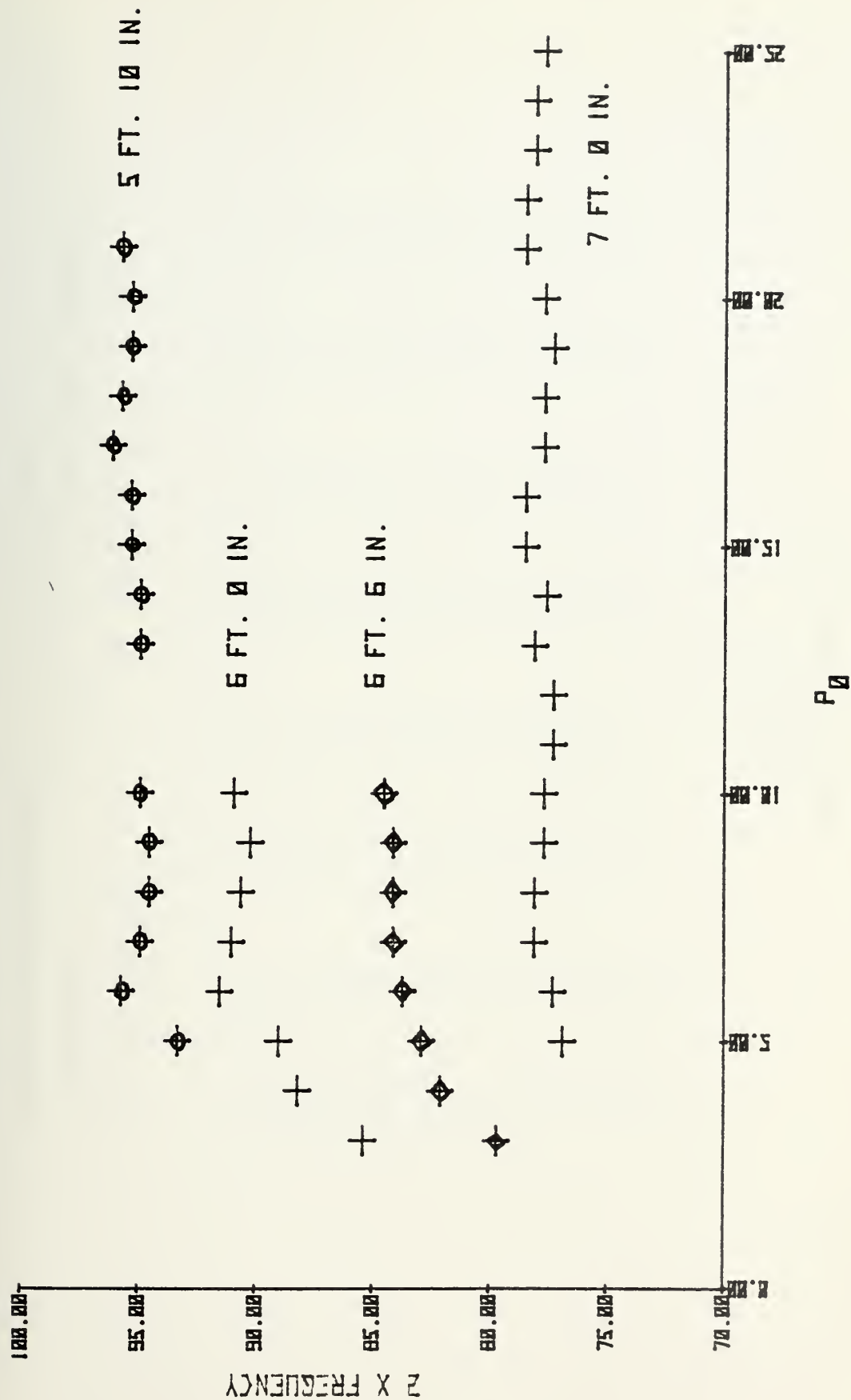
Figure 11. Frequency of oscillation vs stagnation pressure for present configuration

NOZZLE NO. 2 P_A = 30.31 In. Hg

THREE INCHES FROM EXIT T = 60 DEG. F

OSCILLATING X = INCHES FROM CENTERLINE

F_0 = 10 In. Hg P = In. Hg

X	P	X	P	X	P	X	P
-2.00	0.0	-1.90	0.0	-1.80	0.0	-1.70	0.0
-1.60	0.0	-1.50	0.01	-1.40	0.03	-1.30	0.03
-1.20	0.03	-1.10	0.03	-1.00	0.03	-0.90	0.06
-0.80	0.11	-0.70	0.21	-0.60	0.31	-0.50	0.58
-0.40	0.95	-0.30	1.36	-0.20	1.79	-0.10	2.18
0.0	2.37	0.10	2.52	0.20	2.53	0.30	2.51
0.40	2.38	0.50	2.05	0.60	1.62	0.70	1.20
0.80	0.78	0.90	0.50	1.00	0.30	1.10	0.18
1.20	0.10	1.30	0.06	1.40	0.04	1.50	0.02
1.60	0.0	1.70	0.0	1.80	0.0	1.90	0.0
2.00	0.0						

TABLE XI

Velocity Profile Data

NOZZLE NO. 3 P_A = 30.31 In. Hg

THREE INCHES FROM EXIT   T = 60 DEG. F

OSCILLATING   X = INCHES FROM CENTERLINE

P_O = 10 In. Hg   P = In. Hg

X	P	X	P	X	P	X	P
-2.00	0.0	-1.90	0.0	-1.80	0.0	-1.70	0.0
-1.60	0.0	-1.50	0.0	-1.40	0.01	-1.30	0.05
-1.20	0.09	-1.10	0.19	-1.00	0.36	-0.90	0.73
-0.80	1.09	-0.70	1.50	-0.60	1.77	-0.50	1.75
-0.40	1.50	-0.30	1.11	-0.20	0.79	-0.10	0.55
0.0	0.49	0.10	0.60	0.20	1.00	0.30	1.48
0.40	1.90	0.50	2.00	0.60	1.77	0.70	1.24
0.80	0.84	0.90	0.57	1.00	0.34	1.10	0.19
1.20	0.11	1.30	0.08	1.40	0.05	1.50	0.0
1.60	0.0	1.70	0.0	1.80	0.0	1.90	0.0
2.00	0.0						

TABLE XII

Velocity Profile Data

NOZZLE NO. 4

THREE INCHES FROM EXIT

OSCILLATING

P_O = 10 In. Hg

P_A = 30.31 In. Hg

T = 60 DEG. F

X = INCHES FROM CENTERLINE

P = In. Hg

X	P	X	P	X	P	X	P
-2.00	0.0	-1.90	0.0	-1.80	0.0	-1.70	0.0
-1.60	0.0	-1.50	0.0	-1.40	0.0	-1.30	0.0
-1.20	0.0	-1.10	0.0	-1.00	0.0	-0.90	0.01
-0.80	0.06	-0.70	0.13	-0.60	0.28	-0.50	0.55
-0.40	0.87	-0.30	1.25	-0.20	1.59	-0.10	1.80
0.0	1.84	0.10	1.78	0.20	1.66	0.30	1.65
0.40	1.70	0.50	1.68	0.60	1.58	0.70	1.36
0.80	1.10	0.90	0.80	1.00	0.51	1.10	0.32
1.20	0.20	1.30	0.10	1.40	0.07	1.50	0.03
1.60	0.0	1.70	0.0	1.80	0.0	1.90	0.0
2.00	0.0						

TABLE XIII

Velocity Profile Data

51

NOZZLE NO. 2

THREE INCHES FROM EXIT

NON-OSCILLATING

P_0 = 10 In. Hg

P_A = 30.03 In. Hg

T = 69 DEG. F

X = INCHES FROM CENTERLINE

P = In. Hg

X	P	X	P	X	P	X	P
-2.00	0.0	-1.90	0.0	-1.80	0.0	-1.70	0.0
-1.60	0.0	-1.50	0.0	-1.40	0.0	-1.30	0.0
-1.20	0.0	-1.10	0.0	-1.00	0.01	-0.90	0.02
-0.80	0.03	-0.70	0.03	-0.60	0.05	-0.50	0.10
-0.40	0.23	-0.30	0.66	-0.20	1.30	-0.10	2.28
0.0	3.44	0.10	4.38	0.20	4.48	0.30	3.75
0.40	2.75	0.50	1.62	0.60	0.95	0.70	0.41
0.80	0.20	0.90	0.10	1.00	0.05	1.10	0.03
1.20	0.02	1.30	0.0	1.40	0.0	1.50	0.0
1.60	0.0	1.70	0.0	1.80	0.0	1.90	0.0
2.00	0.0						

TABLE XIV

Velocity Profile Data

NOZZLE NO. 3

THREE INCHES FROM EXIT

NON-OSCILLATING

P_0 = 10 In. Hg

P_A = 30.03 In. Hg

T = 69 DEG. F

X = INCHES FROM CENTERLINE

P = In. Hg

X	P	X	P	X	P	X	P
-2.00	0.0	-1.90	0.0	-1.80	0.0	-1.70	0.0
-1.60	0.0	-1.50	0.0	-1.40	0.0	-1.30	0.0
-1.20	0.0	-1.10	0.0	-1.00	0.0	-0.90	0.0
-0.80	0.01	-0.70	0.01	-0.60	0.01	-0.50	0.02
-0.40	0.04	-0.30	0.12	-0.20	0.39	-0.10	1.02
0.0	2.30	0.10	3.45	0.20	4.57	0.30	4.50
0.40	3.54	0.50	2.22	0.60	1.12	0.70	0.51
0.80	0.22	0.90	0.09	1.00	0.04	1.10	0.02
1.20	0.01	1.30	0.0	1.40	0.0	1.50	0.0
1.60	0.0	1.70	0.0	1.80	0.0	1.90	0.0
2.00	0.0						

TABLE XV

Velocity Profile Data

NOZZLE NO. 4 P_A = 30.03 In. Hg

THREE INCHES FROM EXIT   T = 69 DEG. F

NON-OSCILLATING   X = INCHES FROM CENTERLINE

P_O = 10 In. Hg   P = In. Hg

X	P	X	P	X	P	X	P
-2.00	0.0	-1.90	0.0	-1.80	0.0	-1.70	0.0
-1.60	0.0	-1.50	0.0	-1.40	0.0	-1.30	0.0
-1.20	0.0	-1.10	0.0	-1.00	0.01	-0.90	0.02
-0.80	0.03	-0.70	0.03	-0.60	0.07	-0.50	0.12
-0.40	0.42	-0.30	0.93	-0.20	1.67	-0.10	2.73
0.0	3.60	0.10	3.96	0.20	3.46	0.30	2.35
0.40	1.56	0.50	0.72	0.60	0.31	0.70	0.13
0.80	0.07	0.90	0.04	1.00	0.02	1.10	0.01
1.20	0.0	1.30	0.0	1.40	0.0	1.50	0.0
1.60	0.0	1.70	0.0	1.80	0.0	1.90	0.0
2.00	0.0						

TABLE XVI

Velocity Profile Data

NOZZLE NO. 2

NINE INCHES FROM EXIT

OSCILLATING

P_0 = 10 In. Hg

F_A = 29.98 In. Hg

T = 59 DEG. F

X = INCHES FROM CENTERLINE

P = In. Hg

X	P	X	P	X	P	X	P
-4.00	0.0	-3.80	0.0	-3.60	0.0	-3.40	0.0
-3.20	0.0	-3.00	0.0	-2.80	0.01	-2.60	0.02
-2.40	0.05	-2.20	0.09	-2.00	0.12	-1.80	0.17
-1.60	0.23	-1.40	0.29	-1.20	0.35	-1.00	0.43
-0.80	0.47	-0.60	0.53	-0.40	0.55	-0.20	0.57
0.0	0.58	0.20	0.58	0.40	0.57	0.60	0.56
0.80	0.55	1.00	0.52	1.20	0.48	1.40	0.41
1.60	0.34	1.80	0.27	2.00	0.20	2.20	0.15
2.40	0.10	2.60	0.06	2.80	0.03	3.00	0.01
3.20	0.0	3.40	0.0	3.60	0.0	3.80	0.0
4.00	0.0						

TABLE XVII

Velocity Profile Data

NOZZLE NO. 3 P_A = 30.18 In. Hg

NINE INCHES FROM EXIT   T = 60 DEG. F

OSCILLATING   X = INCHES FROM CENTERLINE

P_0 = 10 In. Hg   P = In. Hg

X	P	X	P	X	P	X	P
-4.00	0.0	-3.80	0.0	-3.60	0.0	-3.40	0.01
-3.20	0.04	-3.00	0.08	-2.80	0.12	-2.60	0.18
-2.40	0.25	-2.20	0.34	-2.00	0.42	-1.80	0.50
-1.60	0.55	-1.40	0.58	-1.20	0.58	-1.00	0.56
-0.80	0.52	-0.60	0.49	-0.40	0.45	-0.20	0.44
0.0	0.44	0.20	0.45	0.40	0.48	0.60	0.53
0.80	0.58	1.00	0.61	1.20	0.60	1.40	0.57
1.60	0.55	1.80	0.49	2.00	0.39	2.20	0.30
2.40	0.20	2.60	0.13	2.80	0.08	3.00	0.03
3.20	0.01	3.40	0.0	3.60	0.0	3.80	0.0
4.00	0.0						

TABLE XVIII

Velocity Profile Data

NOZZLE NO. 4 P_A = 30.03 In. Hg

NINE INCHES FROM EXIT T = 50 DEG. F

OSCILLATING X = INCHES FROM CENTERLINE

P_0 = 10 In. Hg P = In. Hg

X	P	X	P	X	P	X	P
-4.00	0.0	-3.80	0.0	-3.60	0.0	-3.40	0.0
-3.20	0.01	-3.00	0.01	-2.80	0.02	-2.60	0.03
-2.40	0.05	-2.20	0.10	-2.00	0.14	-1.80	0.17
-1.60	0.21	-1.40	0.26	-1.20	0.33	-1.00	0.38
-0.80	0.44	-0.60	0.47	-0.40	0.52	-0.20	0.55
0.0	0.55	0.20	0.55	0.40	0.52	0.60	0.53
0.80	0.55	1.00	0.54	1.20	0.52	1.40	0.48
1.60	0.45	1.80	0.40	2.00	0.37	2.20	0.32
2.40	0.25	2.60	0.19	2.80	0.14	3.00	0.10
3.20	0.06	3.40	0.04	3.60	0.02	3.80	0.01
4.00	0.0						

TABLE XIX

Velocity Profile Data

NOZZLE NO. 2 P_A = 29.98 In. Hg

NINE INCHES FROM EXIT T = 59 DEG. F

NON-OSCILLATING X = INCHES FROM CENTERLINE

P_0 = 10 In. Hg P = In. Hg

X	P	X	P	X	P	X	P
-4.00	0.0	-3.80	0.0	-3.60	0.0	-3.40	0.0
-3.20	0.0	-3.00	0.0	-2.80	0.0	-2.60	0.0
-2.40	0.0	-2.20	0.0	-2.00	0.0	-1.80	0.0
-1.60	0.02	-1.40	0.09	-1.20	0.17	-1.00	0.31
-0.80	0.48	-0.60	0.73	-0.40	0.99	-0.20	1.25
0.0	1.46	0.20	1.49	0.40	1.36	0.60	1.15
0.80	0.90	1.00	0.69	1.20	0.43	1.40	0.30
1.60	0.17	1.80	0.07	2.00	0.03	2.20	0.01
2.40	0.0	2.60	0.0	2.80	0.0	3.00	0.0
3.20	0.0	3.40	0.0	3.60	0.0	3.80	0.0
4.00	0.0						

TABLE XX

Velocity Profile Data

NOZZLE NO. 3 P_A = 29.98 In. Hg

NINE INCHES FROM EXIT   T = 59 DEG. F

NON-OSCILLATING   X = INCHES FROM CENTERLINE

P_0 = 10 In. Hg   P = In. Hg

X	P	X	P	X	P	X	P
-4.00	0.0	-3.80	0.0	-3.60	0.0	-3.40	0.0
-3.20	0.0	-3.00	0.0	-2.80	0.0	-2.60	0.0
-2.40	0.0	-2.20	0.0	-2.00	0.0	-1.80	0.0
-1.60	0.0	-1.40	0.03	-1.20	0.08	-1.00	0.19
-0.80	0.34	-0.60	0.54	-0.40	0.83	-0.20	1.13
0.0	1.37	0.20	1.48	0.40	1.41	0.60	1.21
0.80	0.92	1.00	0.66	1.20	0.41	1.40	0.25
1.60	0.13	1.80	0.05	2.00	0.01	2.20	0.0
2.40	0.0	2.60	0.0	2.80	0.0	3.00	0.0
3.20	0.0	3.40	0.0	3.60	0.0	3.80	0.0
4.00	0.0						

TABLE XXI

Velocity Profile Data

NOZZLE NO. 4

F_A = 29.98 In. Hg

NINE INCHES FROM EXIT

T = 59 DEG. F

NON-OSCILLATING

X = INCHES FROM CENTERLINE

P_0 = 10 In. Hg

P = In. Hg

X	P	X	P	X	P	X	P
-4.00	0.0	-3.80	0.0	-3.60	0.0	-3.40	0.0
-3.20	0.0	-3.00	0.0	-2.80	0.0	-2.60	0.0
-2.40	0.0	-2.20	0.0	-2.00	0.0	-1.80	0.02
-1.60	0.04	-1.40	0.11	-1.20	0.23	-1.00	0.38
-0.80	0.57	-0.60	0.67	-0.40	1.01	-0.20	1.25
0.0	1.34	0.20	1.27	0.40	1.10	0.60	0.89
0.80	0.66	1.00	0.40	1.20	0.26	1.40	0.14
1.60	0.06	1.80	0.02	2.00	0.0	2.20	0.0
2.40	0.0	2.60	0.0	2.80	0.0	3.00	0.0
3.20	0.0	3.40	0.0	3.60	0.0	3.80	0.0
4.00	0.0						

TABLE XXII

Velocity Profile Data
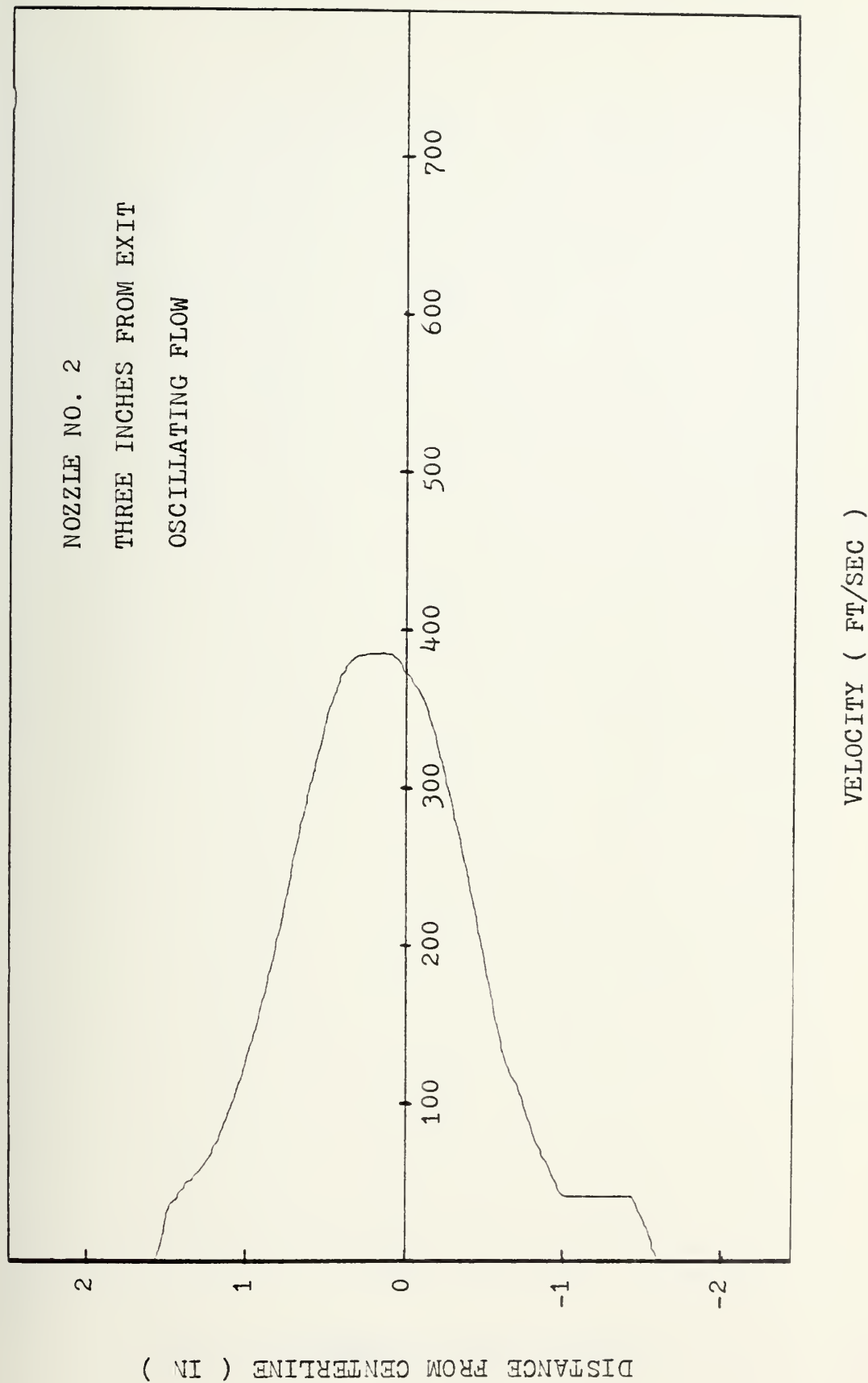
Figure 12. Velocity profile for oscillating flow three inches from exit, nozzle no. 2
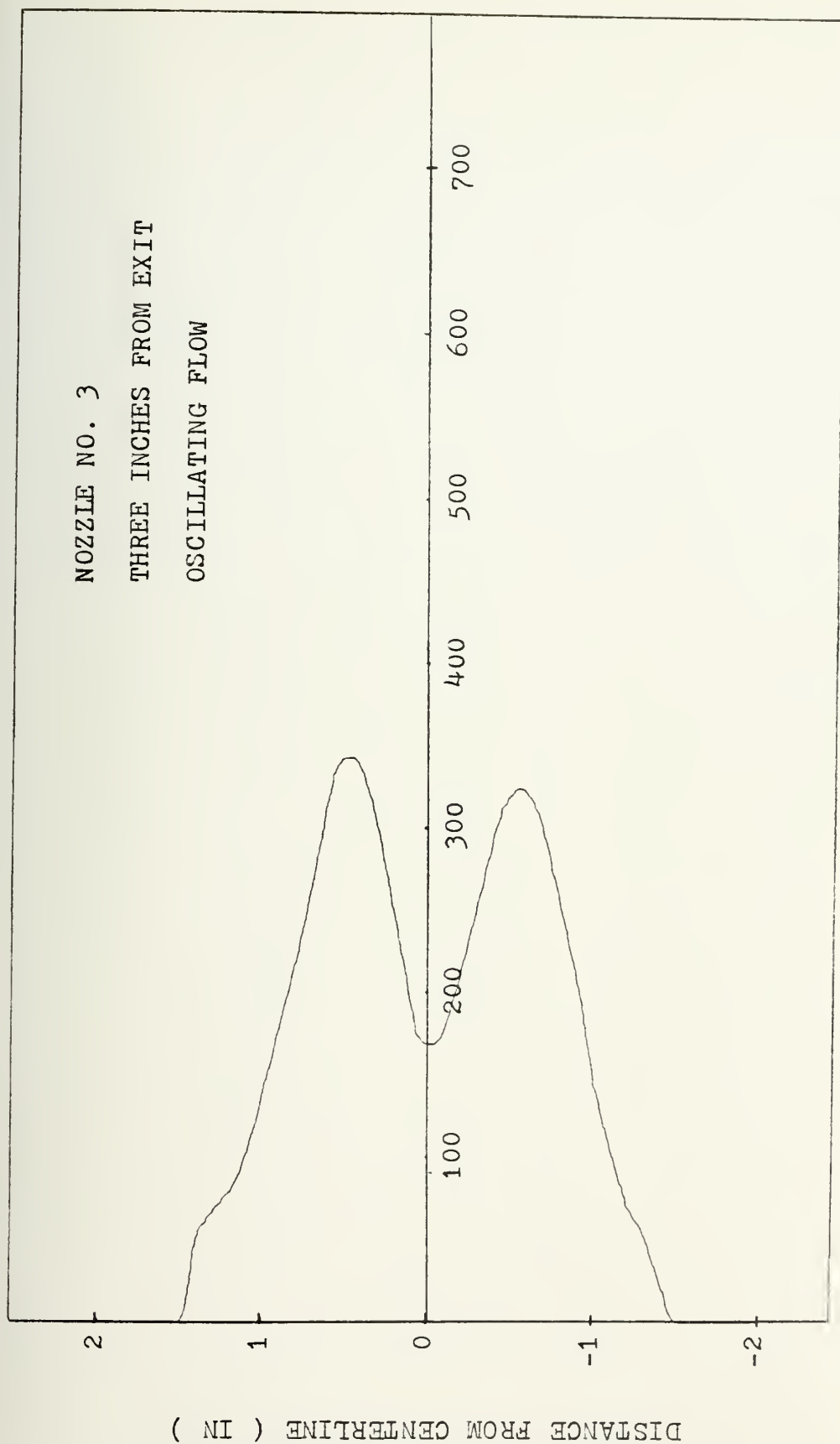
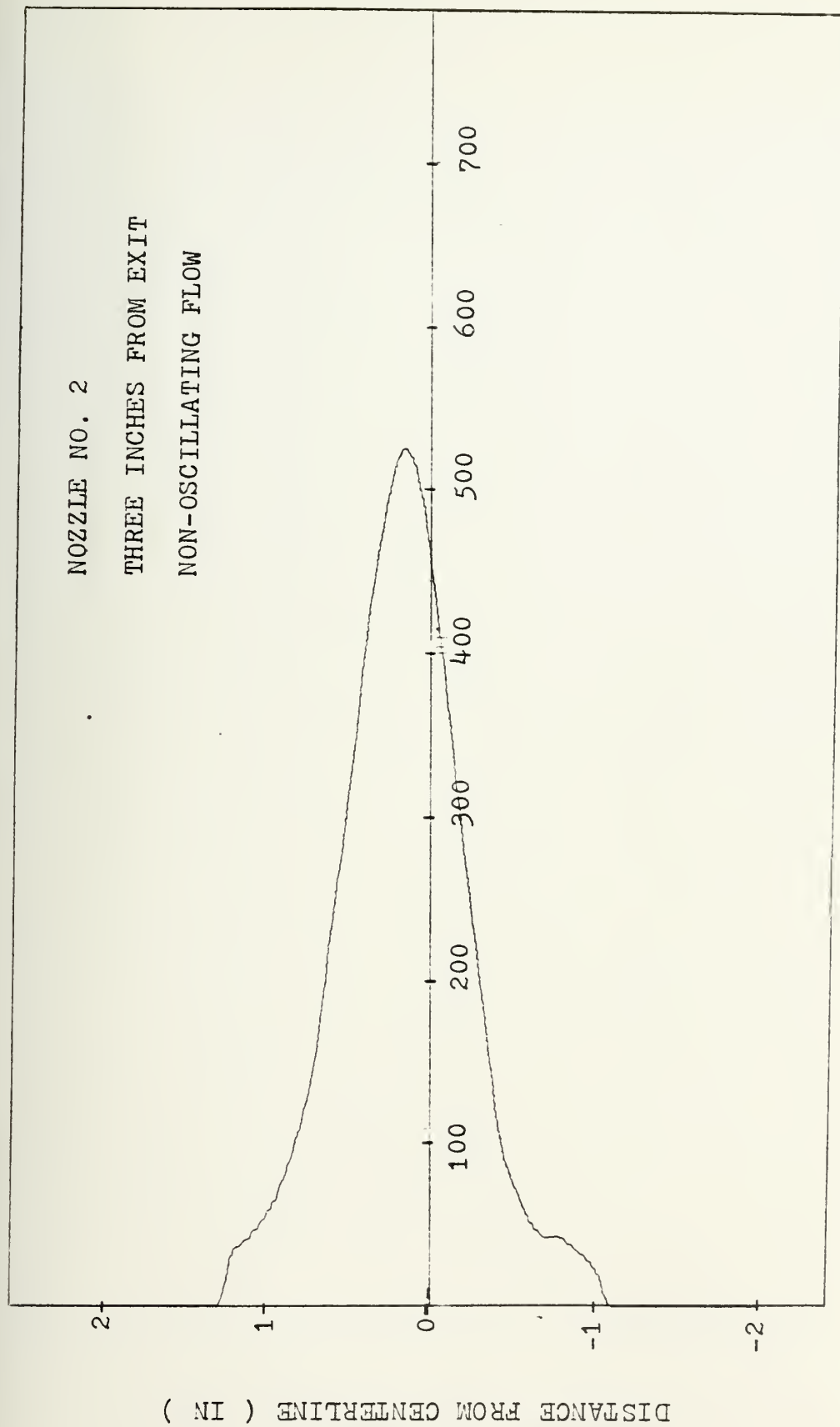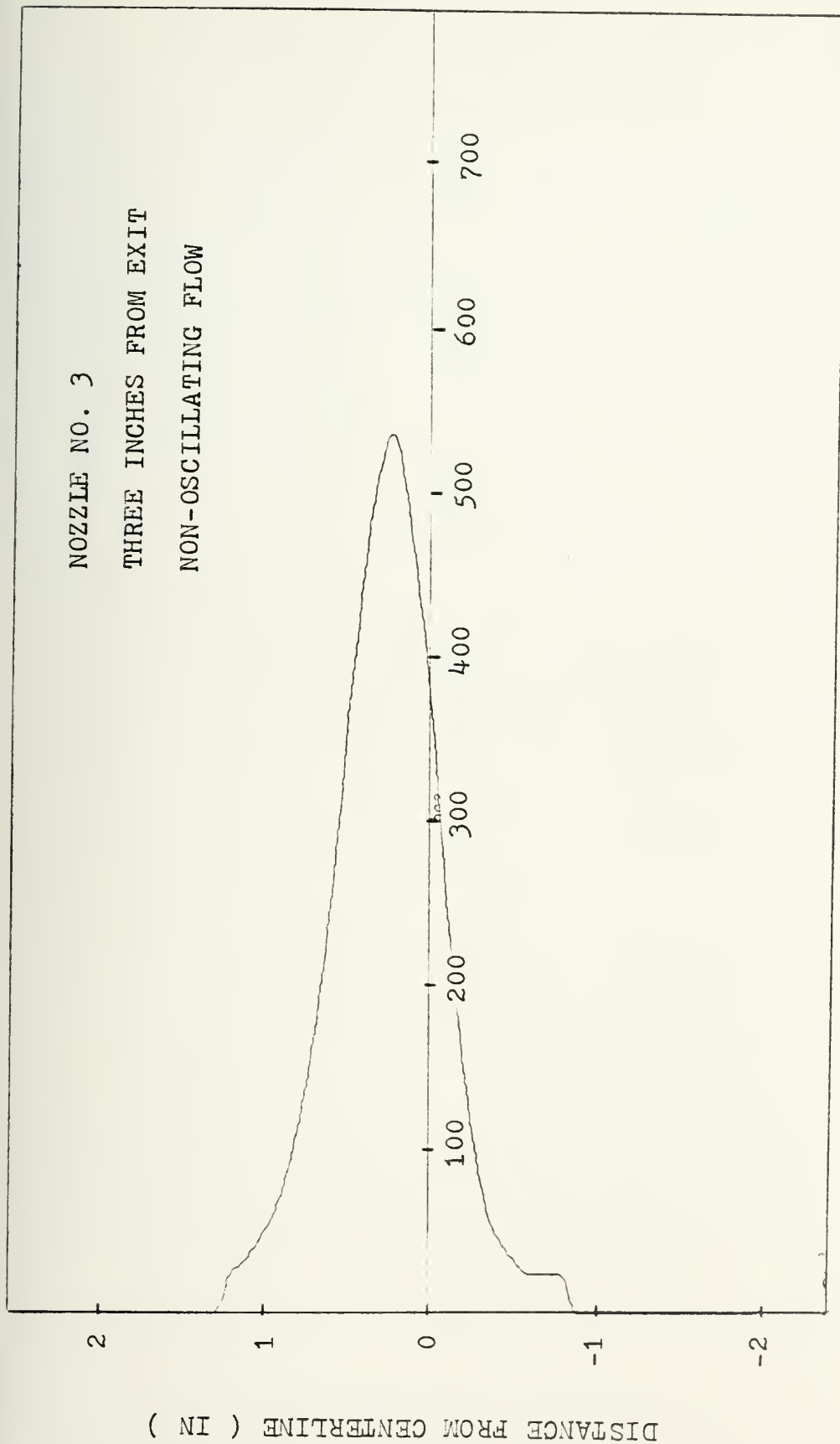Figure 13. Velocity profile for oscillating flow three inches from exit,
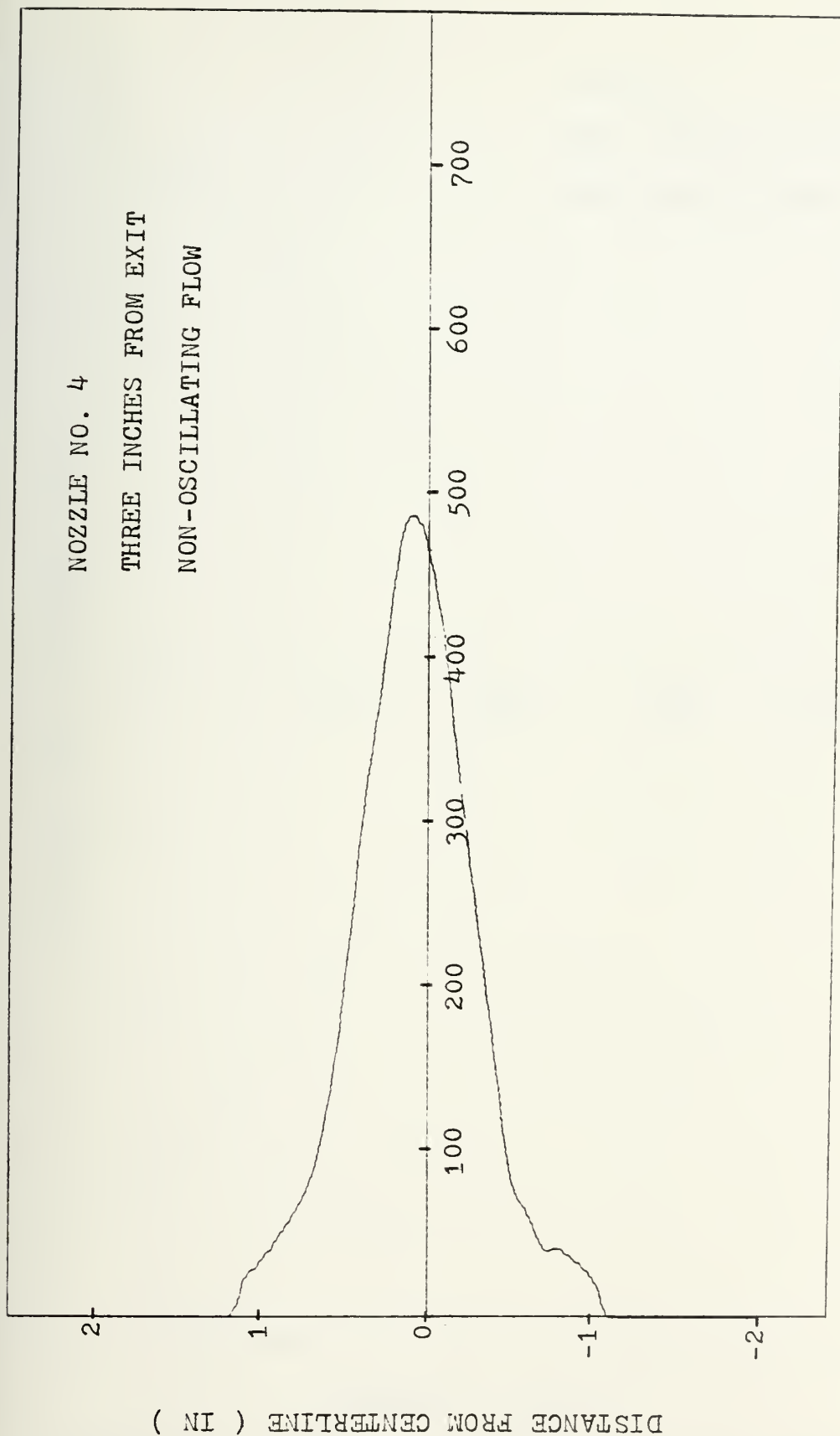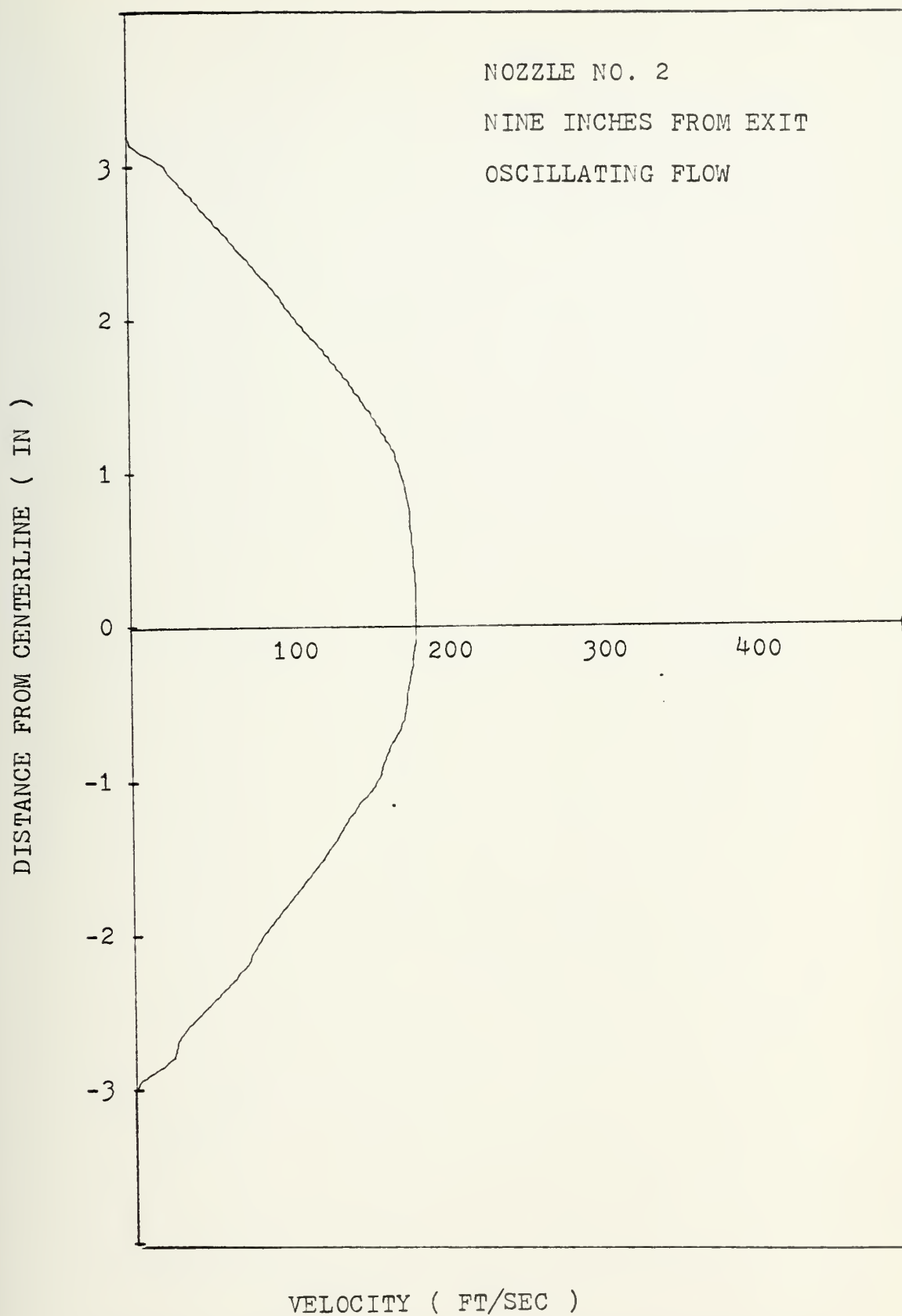nozzle no. 3

NOZZLE NO. 4

THREE INCHES FROM EXIT

OSCILLATING FLOW

VELOCITY (FT/SEC)

DISTANCE FROM CENTERLINE (IN)
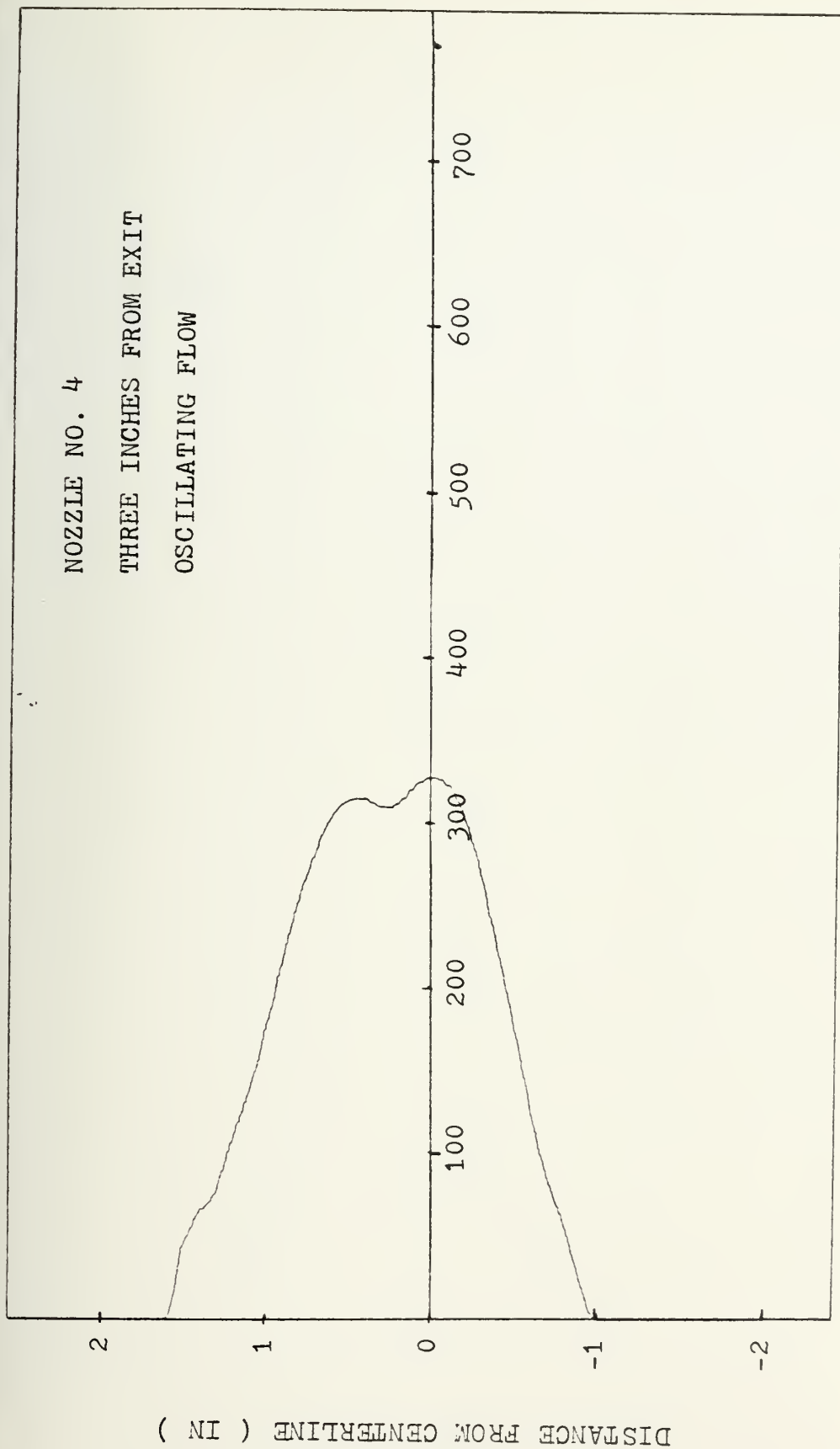
Figure 14. Velocity profile for oscillating flow three inches from exit,
nozzle no. 4

Figure 15. Velocity profile for non-oscillating flow three inches from exit, nozzle no. 2

Figure 16. Velocity profile for non-oscillating flow three inches from exit, nozzle no. 3

Figure 17. Velocity profile for non-oscillating flow three inches from exit, nozzle no. 4

Figure 18.   Velocity profile for oscillating flow
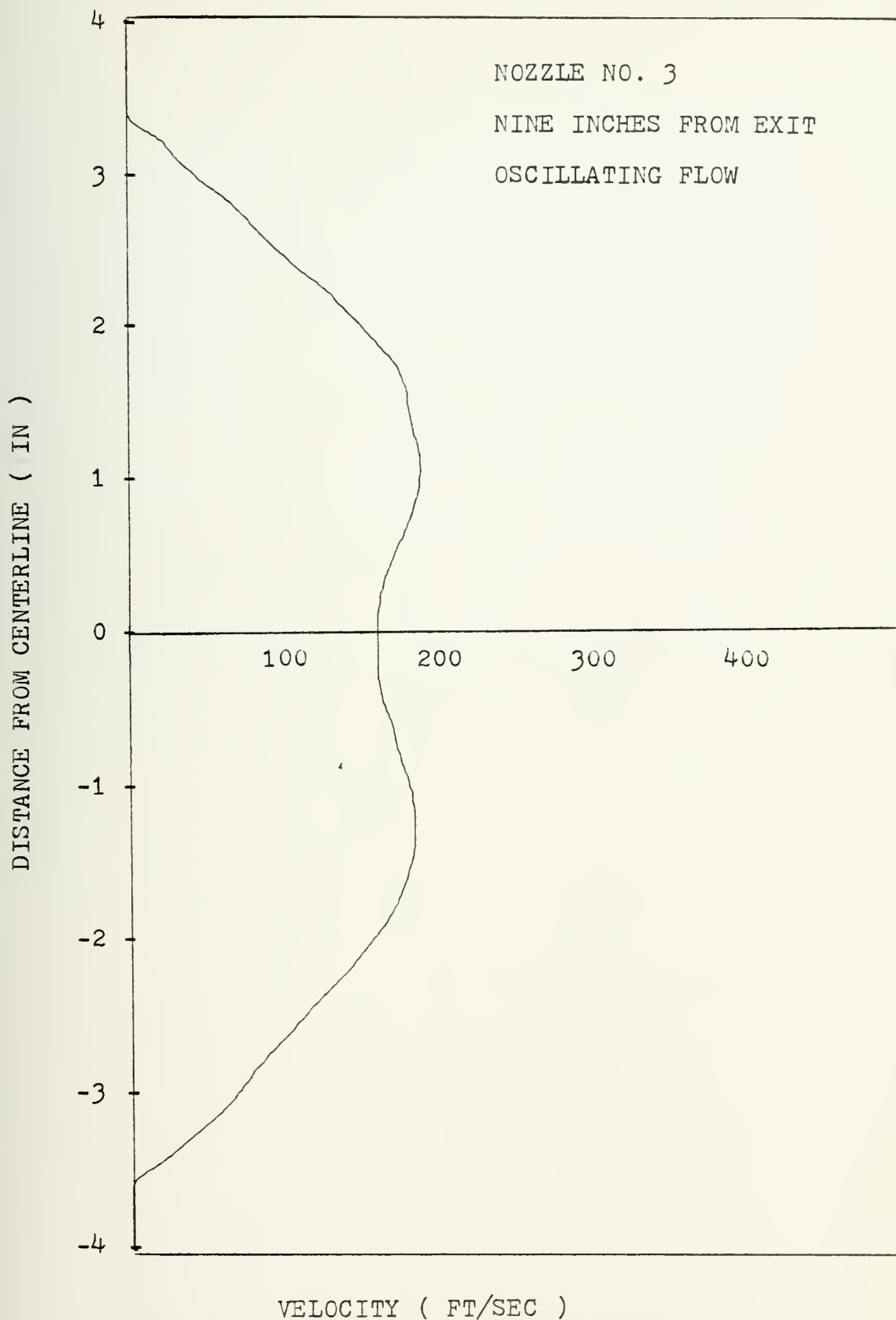nine inches from exit, nozzle no. 2

NOZZLE NO. 3

NINE INCHES FROM EXIT

OSCILLATING FLOW

Figure 19. Velocity profile for oscillating flow
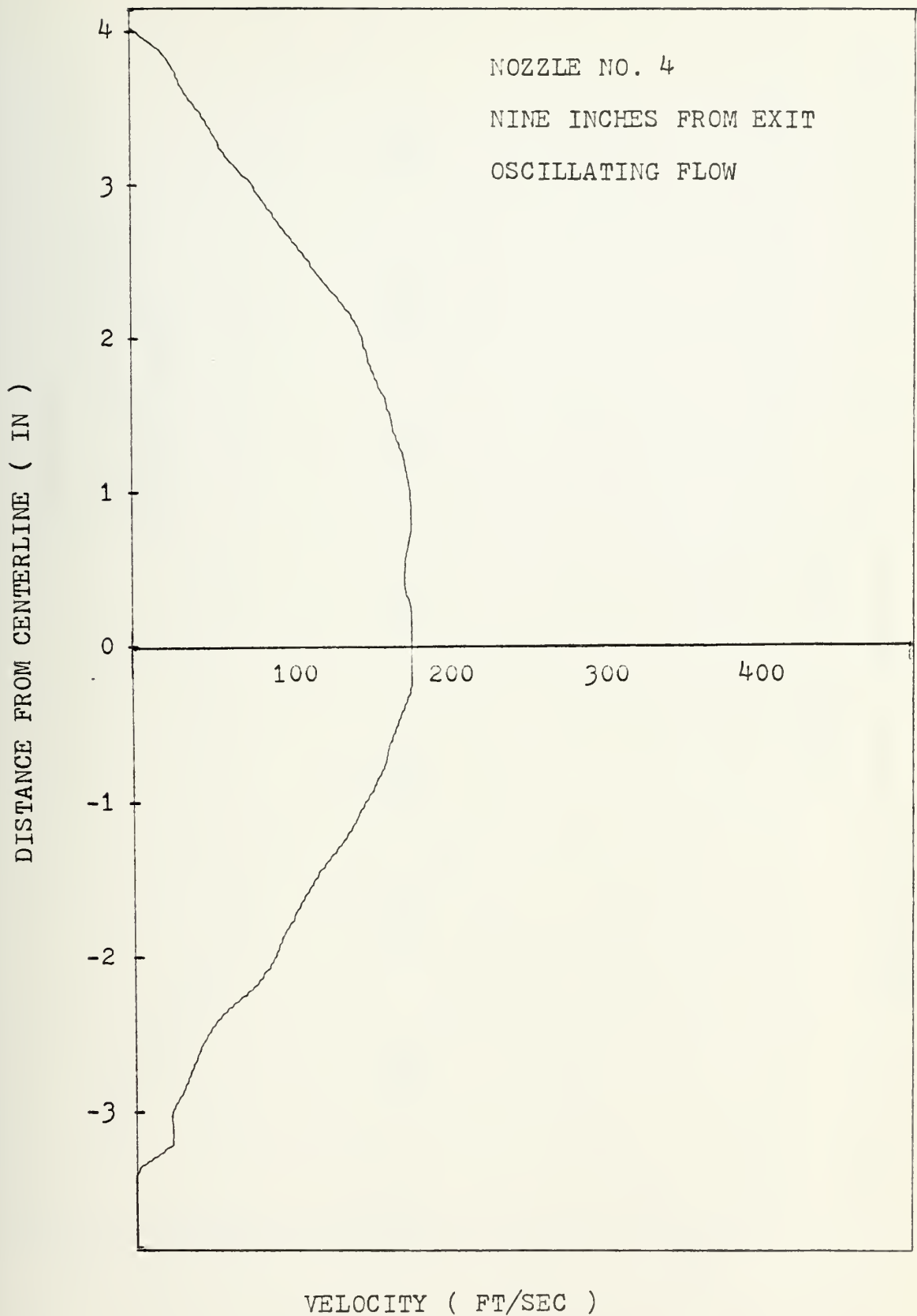nine inches from exit, nozzle no. 3

Figure 20.   Velocity profile for oscillating flow
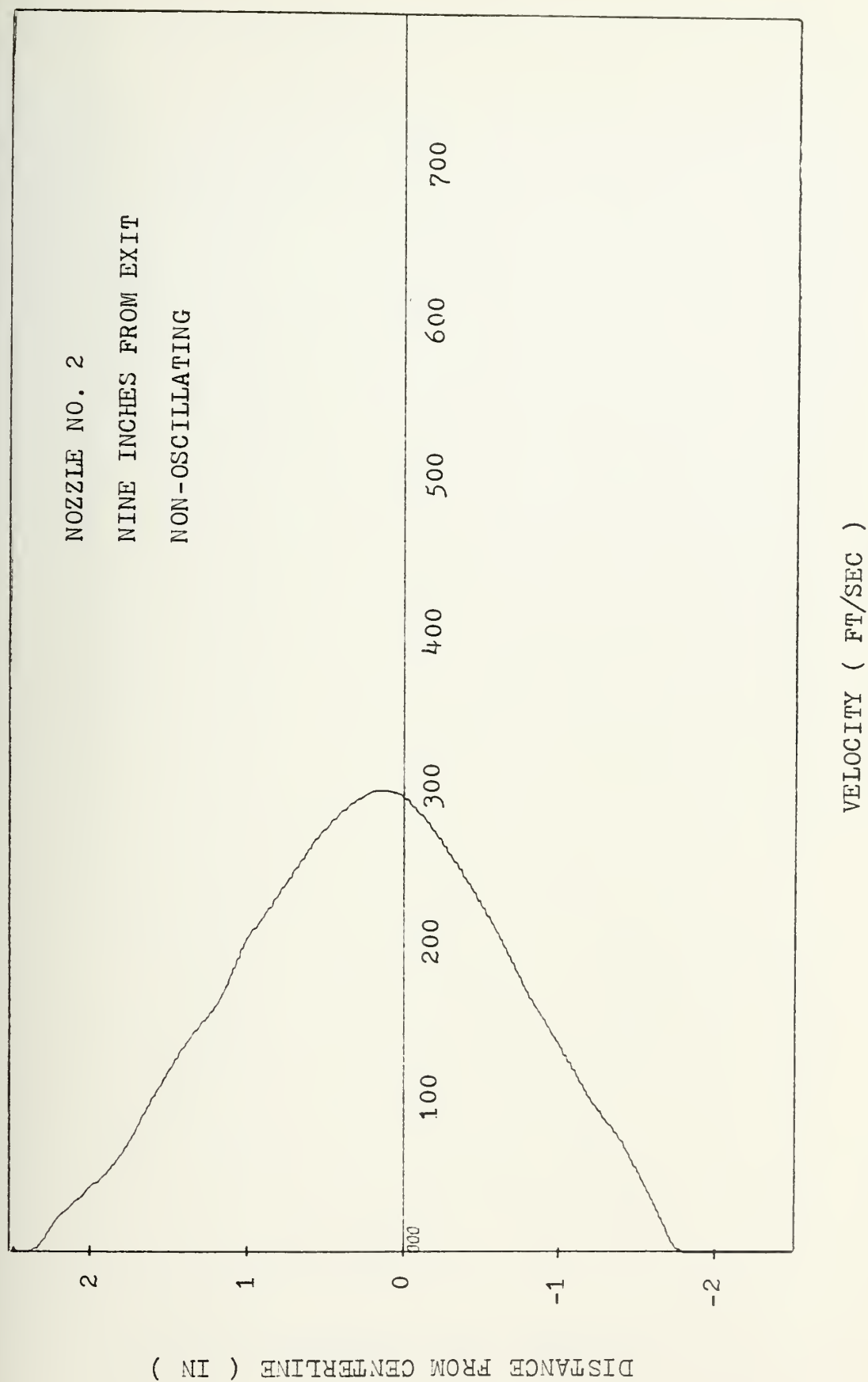nine inches from exit, nozzle no. 4

Figure 21. Velocity profile for non-oscillating flow nine inches from exit, nozzle no. 2
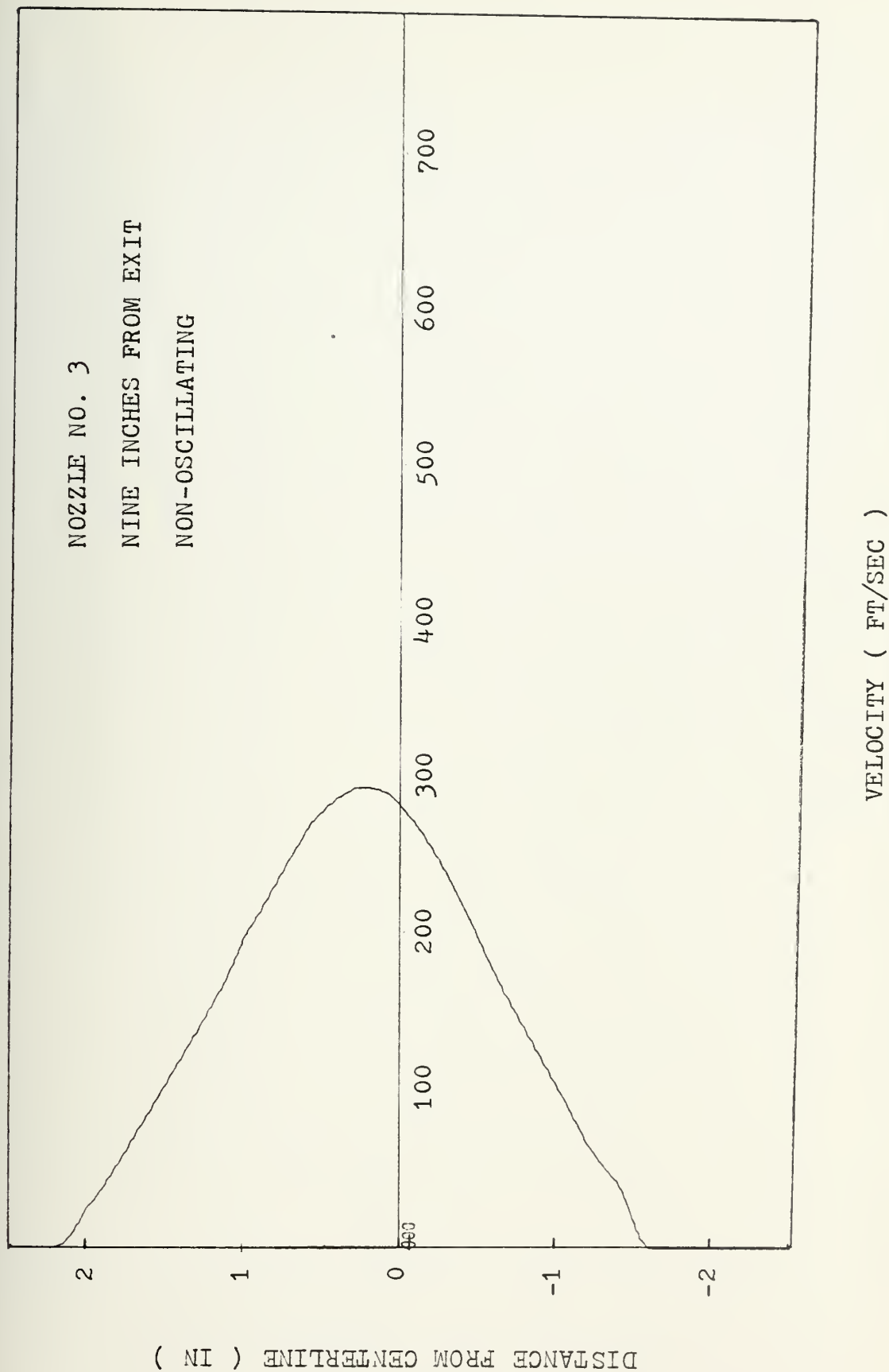
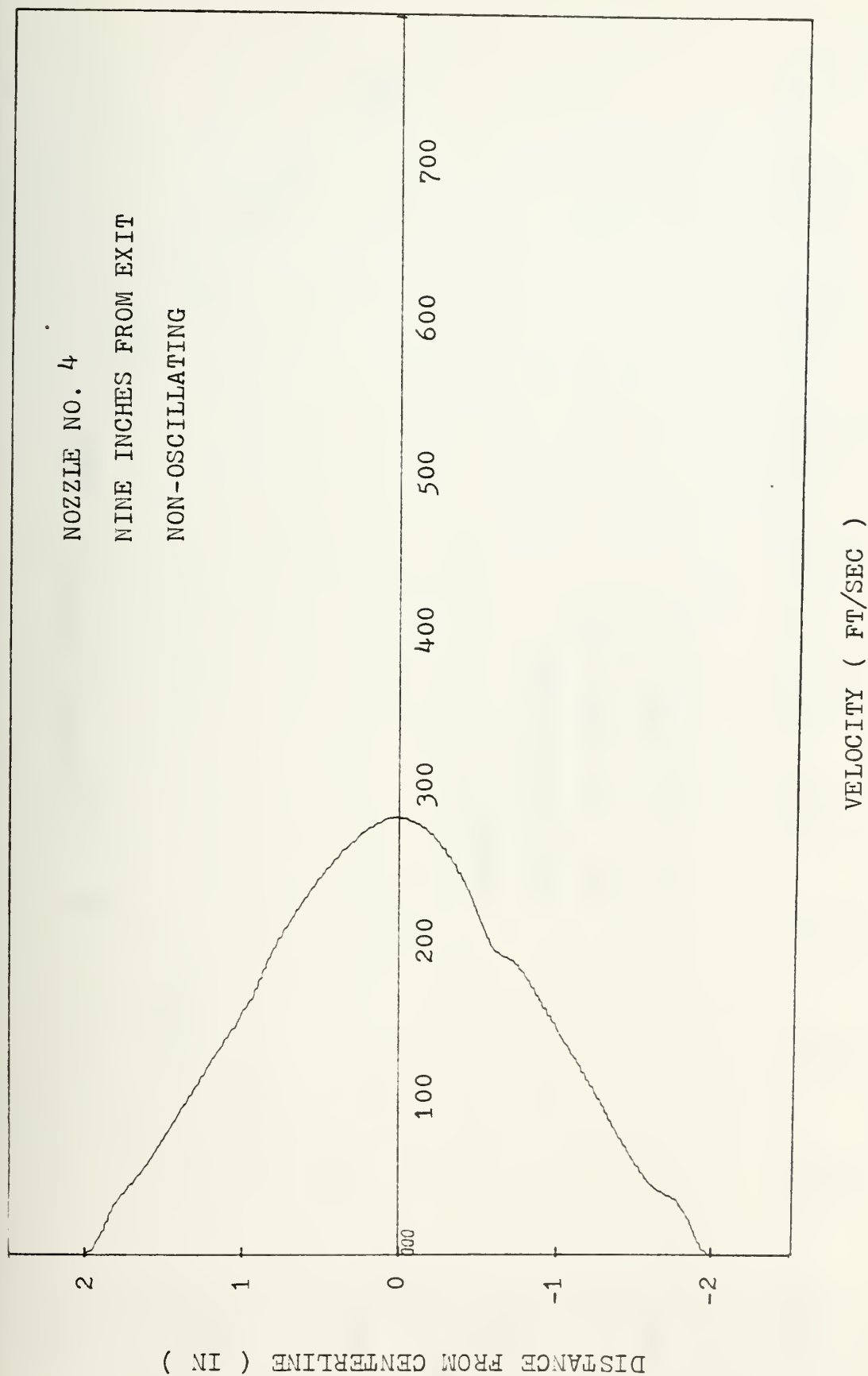Figure 22. Velocity profile for non-oscillating flow nine inches from exit, nozzle no. 3

Figure 23.   Velocity profile for non-oscillating flow nine inches from exit, nozzle no. 4
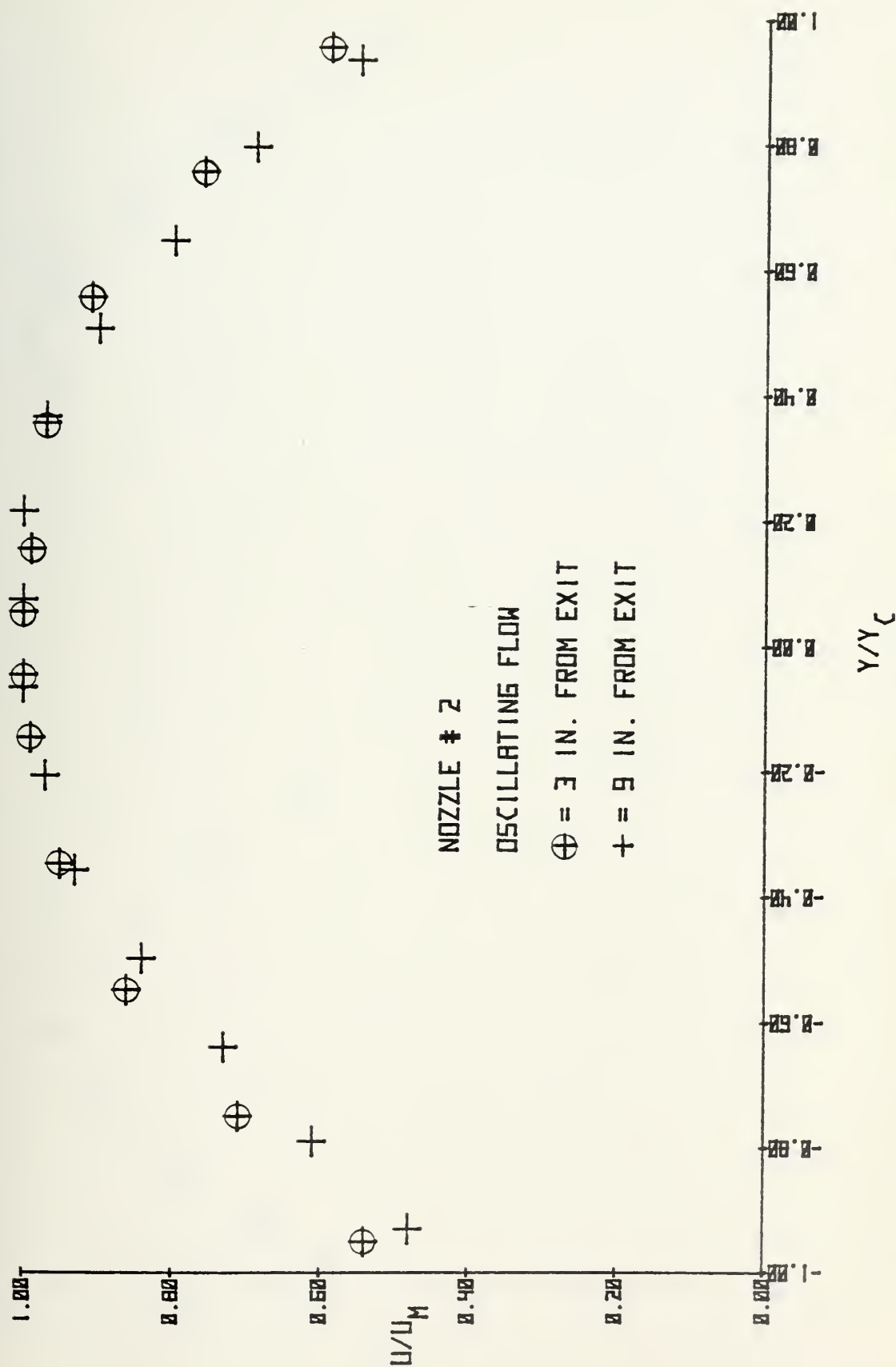
Figure 24. Non-dimensional velocity profile for nozzle no. 2, oscillating flow

Figure 25. Non-dimensional velocity profile for nozzle no. 3, oscillating flow

74

Figure 26.   Non-dimensional velocity profile for nozzle no. 4, oscillating flow
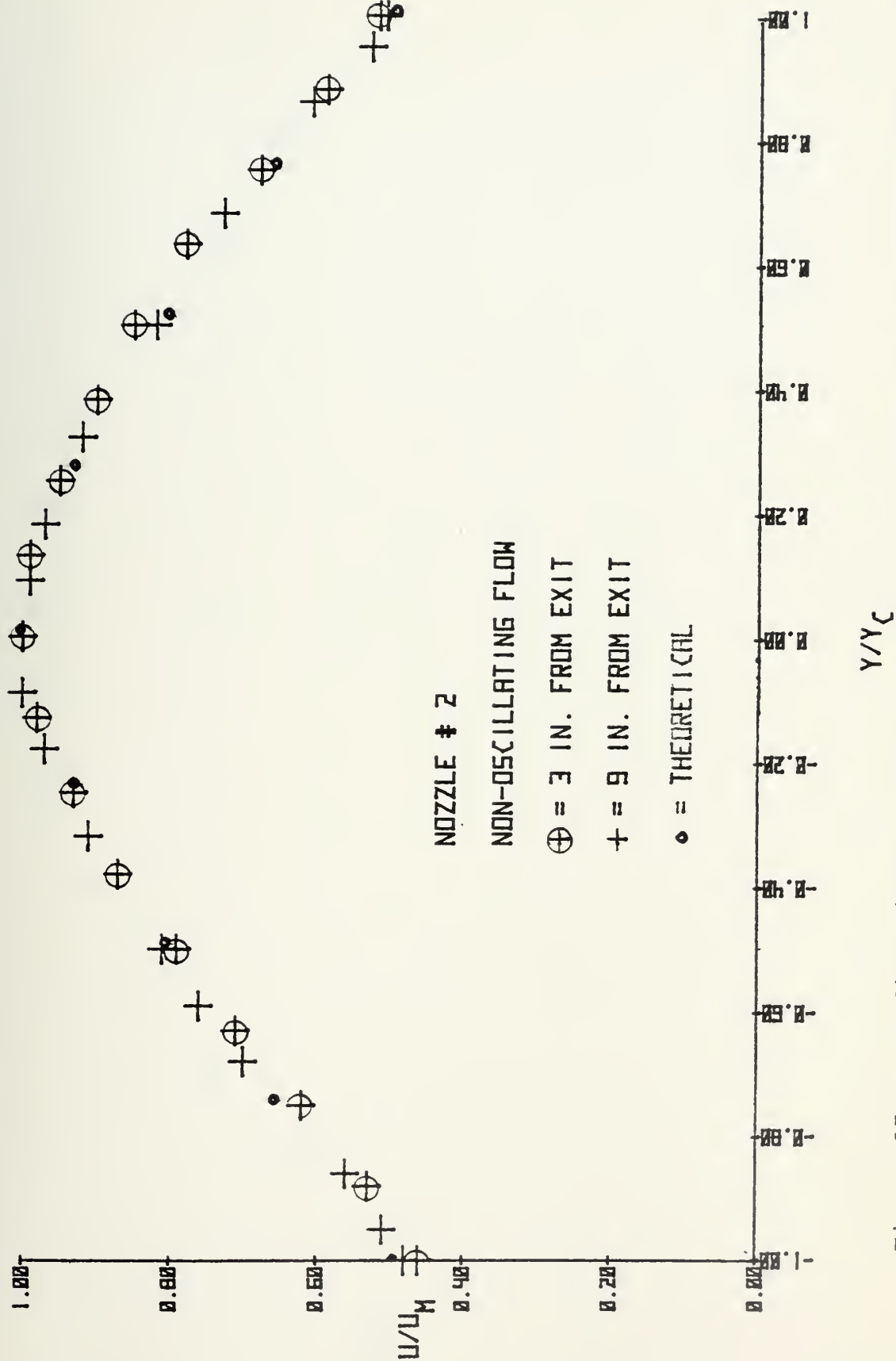
Figure 27. Non-dimensional velocity profile for nozzle no. 2, non-oscillating flow

76
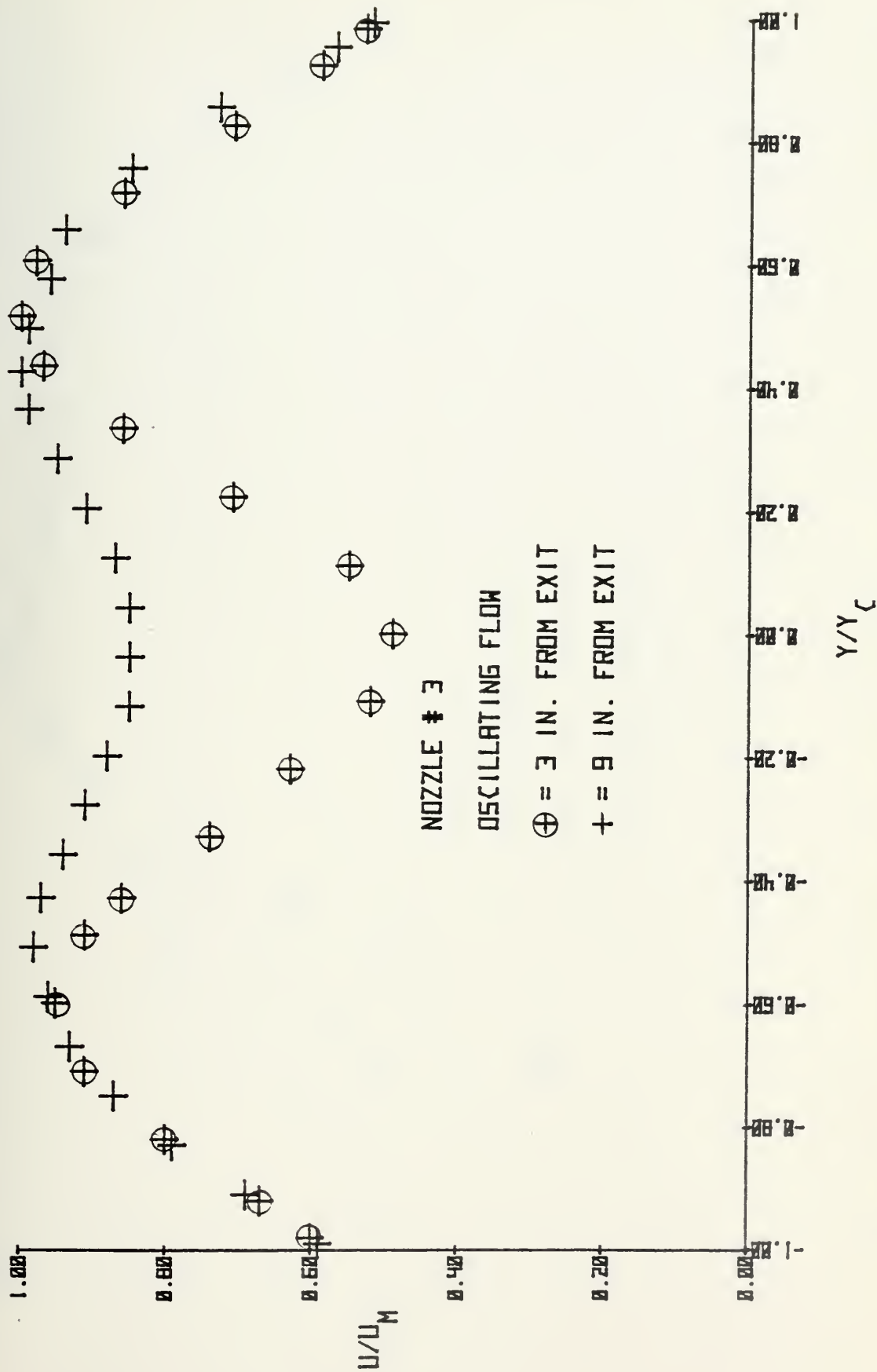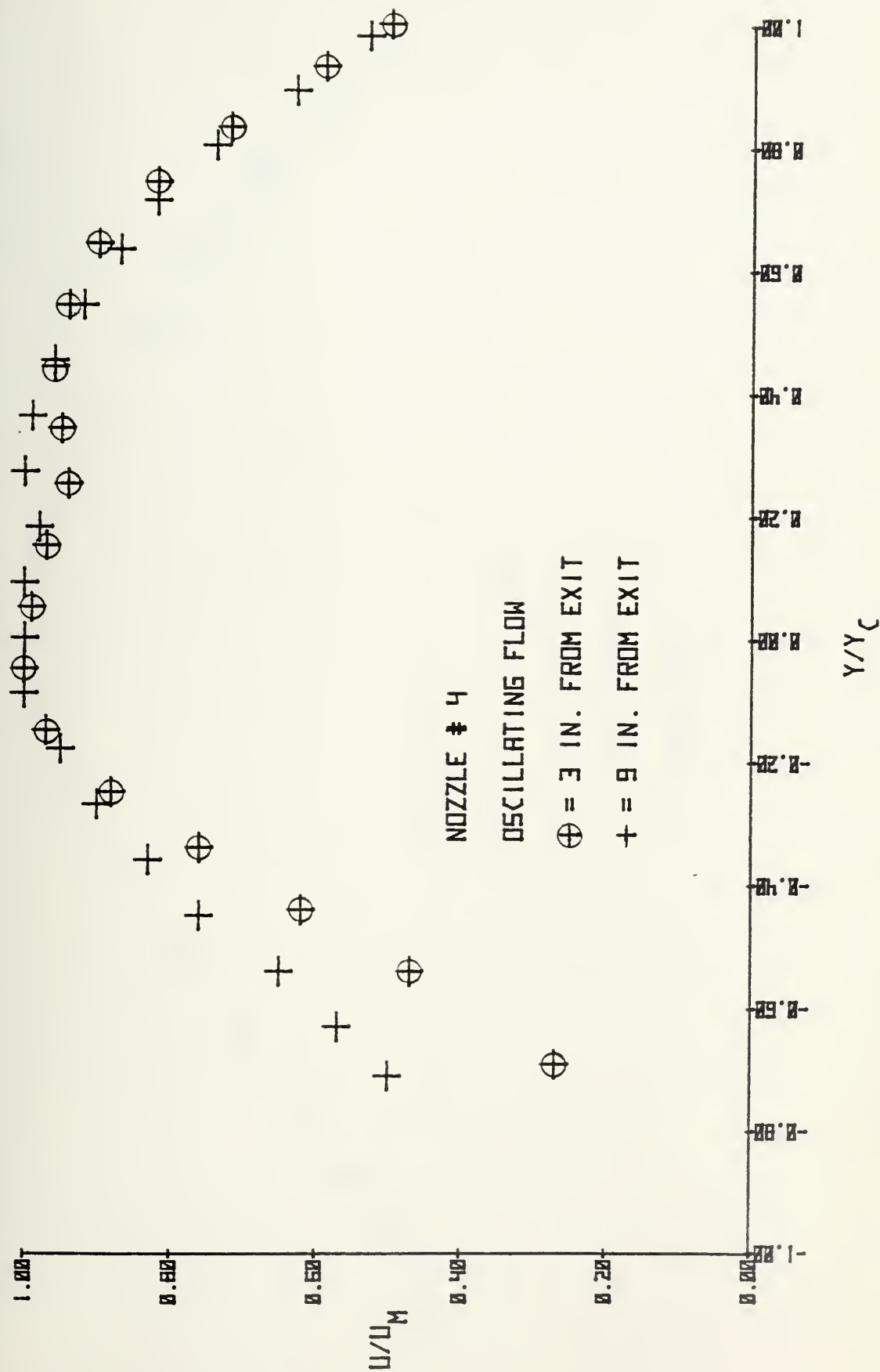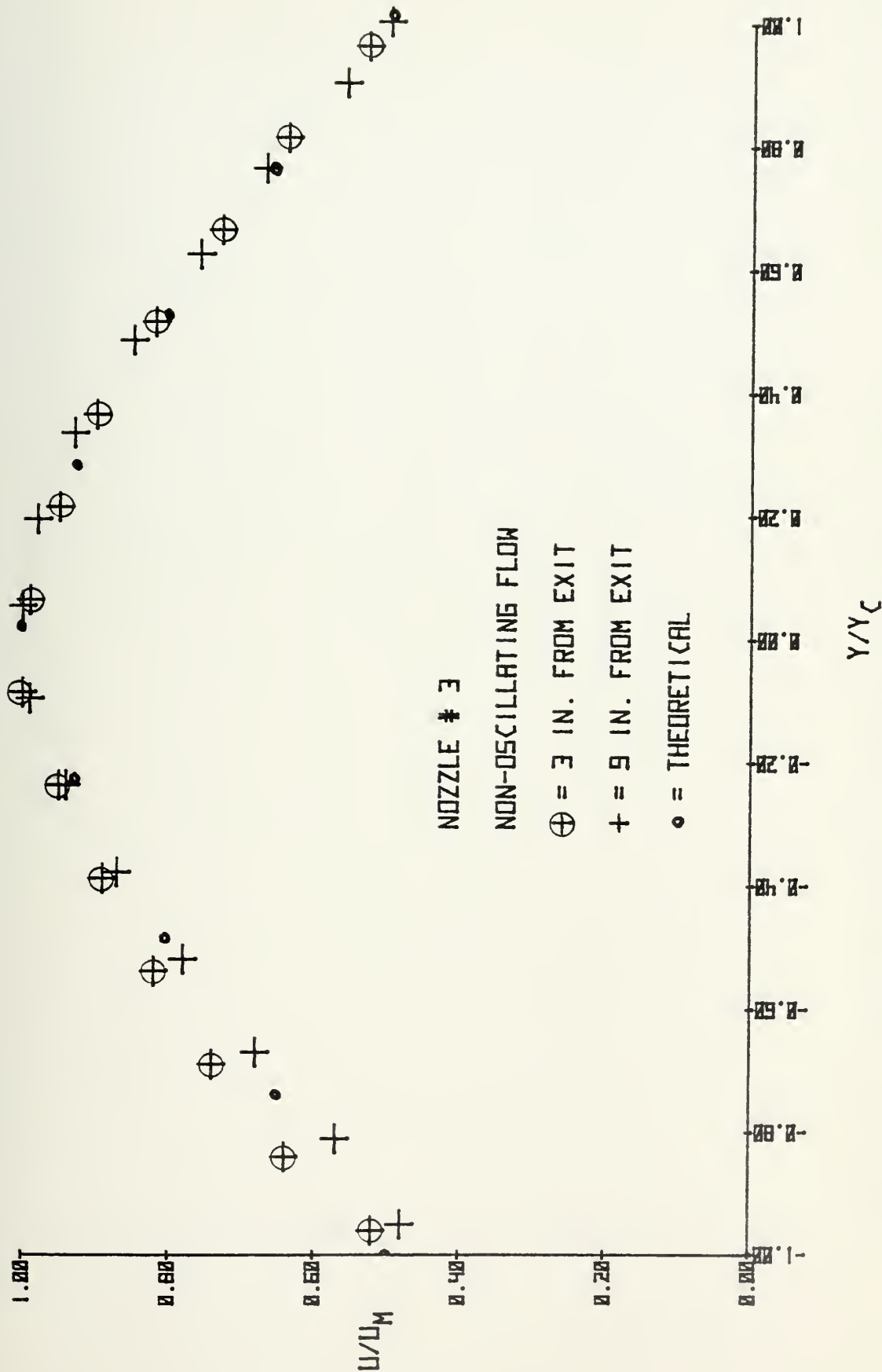
Figure 28.   Non-dimensional velocity profile for nozzle no. 3, non-oscillating flow
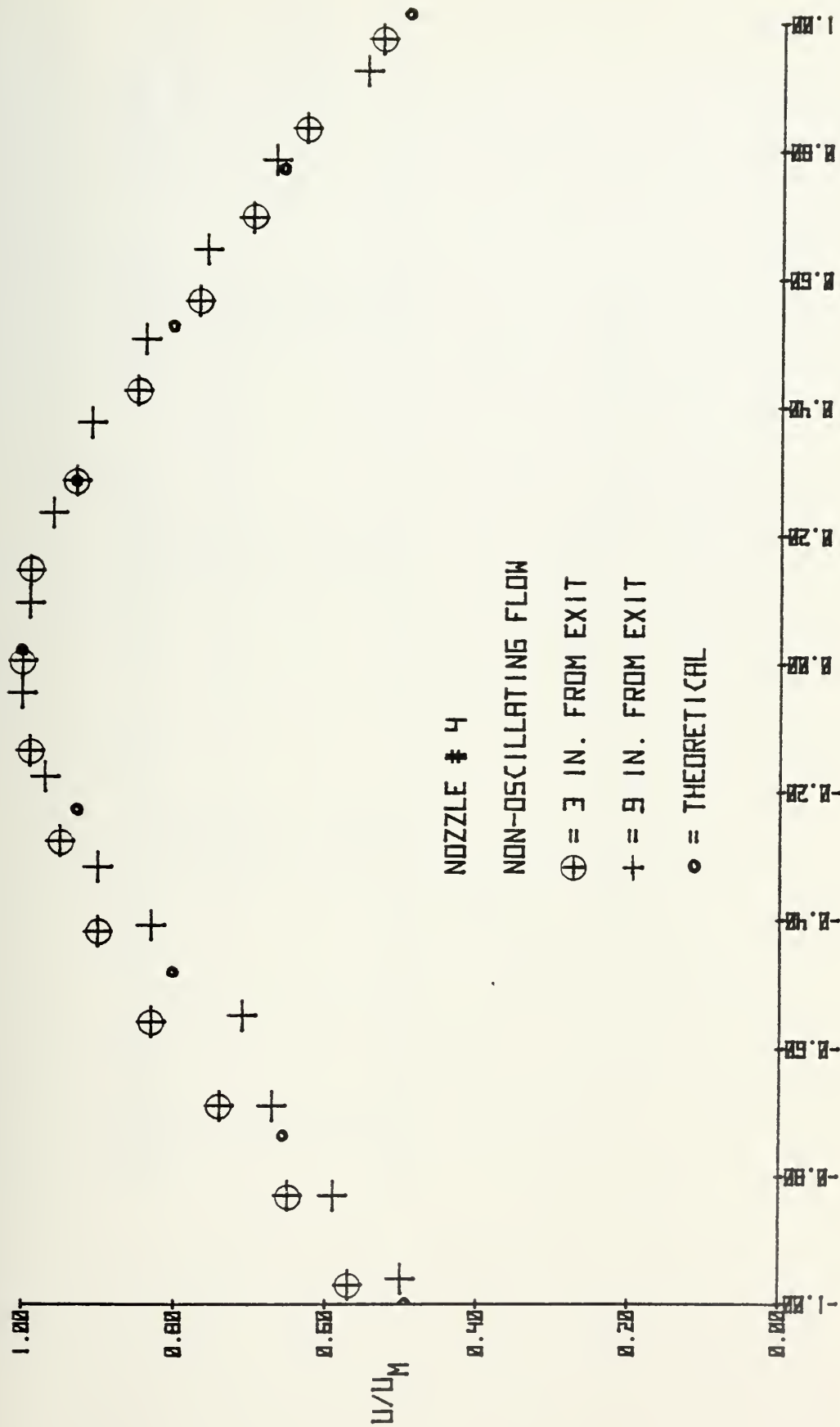
Figure 29. Non-dimensional velocity profile for nozzle no. 4, non-oscillating flow

NOZZLE NO.	NON-OSCILLATING	OSCILLATING	% INCREASE	REMARKS
2	4.65	5.66	21.7	3" from exit
3	4.08	5.83	42.9	"
4	4.13	5.11	23.7	"
2	6.57	7.37	12.2	9" from exit
3	6.04	9.24	53.0	"
4	6.00	8.36	39.3	"

TABLE XXIII

Areas from integrated velocity profiles
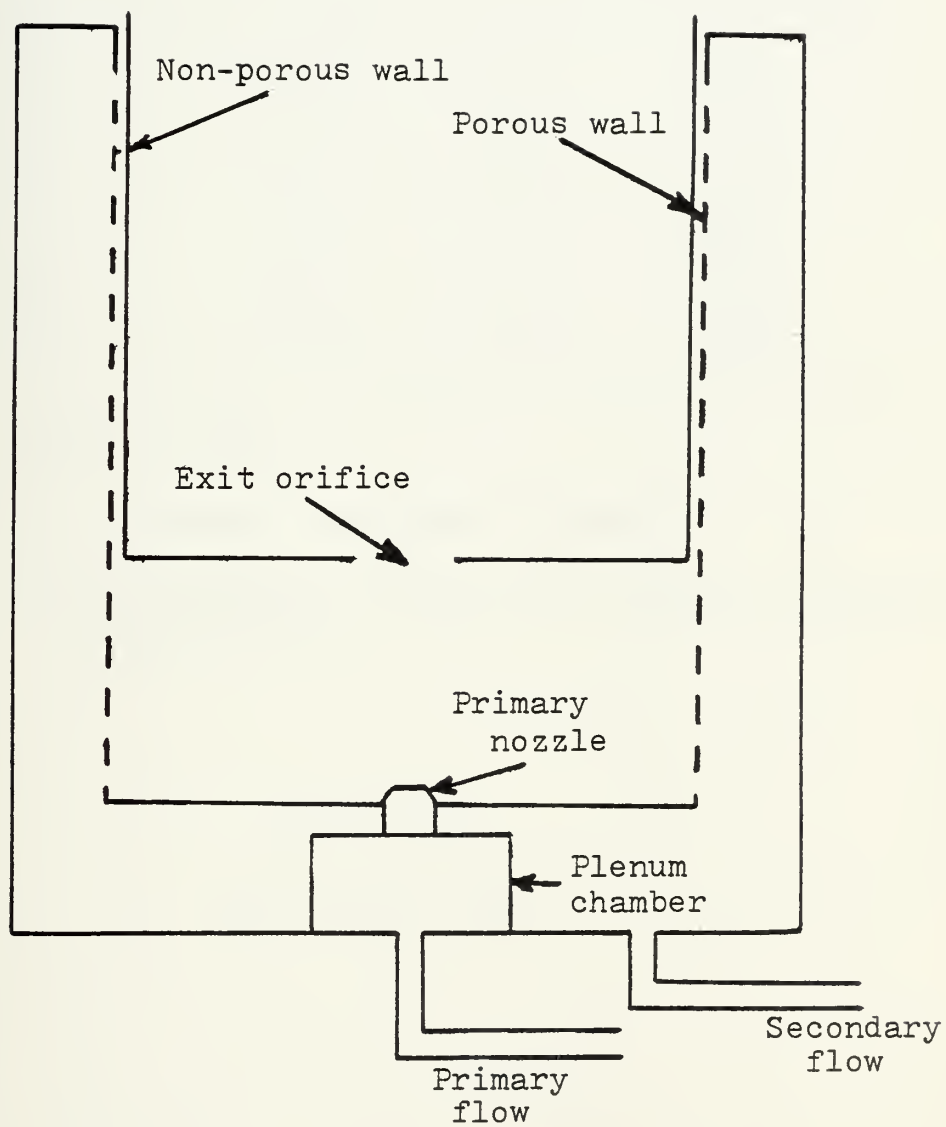
Figure 30. Schematic of entrainment chamber

STEADY FLOW

AXIAL STATION: 3.75 in.

ORIFICE DIAMETER: 1.875 in.

ΔP_v (in. Hg)	h (in.)	$\sqrt{\Delta P_v}$	$P_{chamber}$ $(h - h_{zero})$
3.46	1.7319	1.86	- .0923
3.51	1.7671	1.87	- .0571
3.55	1.7870	1.88	- .0372
3.60	1.8037	1.90	- .0205
3.65	1.8238	1.91	- .0004
3.69	1.8417	1.91	.0175
3.72	1.8623	1.93	.0381

h_{zero} = 1.8242 in.

ΔP_v = Pressure drop across venturi

h = Micromanometer reading for pressure difference across orifice

TABLE XXIV

Entrainment Data

STEADY FLOW

AXIAL STATION: 4.50 in.

ORIFICE DIAMETER: 1.875 in.

ΔP_v (in. Hg)	h (in.)	$\sqrt{\Delta P_v}$	$P_{chamber}$ $(h - h_{zero})$
3.73	1.7613	1.93	− .0678
3.80	1.7976	1.95	− .0315
3.80	1.8017	1.95	− .0274
3.84	1.8105	1.96	− .0186
3.88	1.8247	1.97	− .0044
3.88	1.8276	1.97	− .0015
3.89	1.8362	1.97	.0071
3.92	1.8454	1.98	.0163
3.94	1.8555	1.99	.0264
3.95	1.8708	1.99	.0417

h_{zero} = 1.8291

ΔP_v = Pressure drop across venturi

h = Micromanometer reading for pressure difference across orifice

TABLE XXV

Entrainment Data

STEADY FLOW

AXIAL STATION: 4.75 in.

ORIFICE DIAMETER: 1.875 in.

ΔP_v (in. Hg)	h (in.)	$\sqrt{\Delta P_v}$	$P_{chamber}$ (h - h_{zero})
4.21	1.9747	2.05	.1505
4.10	1.9247	2.02	.1005
4.03	1.8891	2.01	.0649
4.00	1.8558	2.00	.0316
3.93	1.8331	1.98	.0089
3.88	1.8040	1.97	- .0202
3.85	1.7830	1.96	- .0412
3.80	1.7558	1.95	- .0684
3.78	1.7433	1.94	- .0809
3.73	1.7201	1.93	- .1041
3.71	1.6978	1.93	- .1264

h_{zero} = 1.8242 in.

ΔP_v = Pressure drop across venturi

h = Micromanometer reading for pressure
difference across orifice

TABLE XXVI

Entrainment Data

83

STEADY FLOW

AXIAL STATION: 5.00 in.

ORIFICE DIAMETER: 1.875 in.

ΔP_v (in. Hg)	h (in.)	$\sqrt{\Delta P_v}$	$P_{chamber}$ $(h - h_{zero})$
3.70	1.7076	1.92	− .1232
3.72	1.7359	1.93	− .0949
3.75	1.7449	1.94	− .0859
3.77	1.7621	1.94	− .0687
3.78	1.7802	1.94	− .0506
3.80	1.7958	1.95	− .0350
3.83	1.8064	1.96	− .0244
3.86	1.8221	1.97	− .0087
3.88	1.8406	1.97	.0098
3.90	1.8495	1.96	.0187
3.90	1.8548	1.96	.0240

h_{zero} = 1.8308

ΔP_v = pressure drop across venturi

h   = Micromanometer reading for pressure difference across orifice

TABLE XXVII

Entrainment Data

84

STEADY FLOW

AXIAL STATION: 5.75 in.

ORIFICE DIAMETER: 1.875 in.

ΔP_v (in. Hg)	h (in.)	$\sqrt{\Delta P_v}$	$P_{chamber}$ $(h - h_{zero})$
3.50	1.6034	1.87	$-$ .2217
3.61	1.6968	1.90	$-$ .1283
3.70	1.8048	1.92	$-$ .0203
3.75	1.8158	1.94	$-$ .0093
3.79	1.8527	1.95	.0276
3.82	1.8838	1.95	.0587
3.87	1.9113	1.97	.0862
4.02	1.9971	2.00	.1720

h_{zero} = 1.8251 in.

ΔP_v = pressure drop across venturi

h   = Micromanometer reading for pressure
     difference across orifice

TABLE XXVIII
Entrainment Data

STEADY FLOW

AXIAL STATION: 6.75 in.

ORIFICE DIAMETER: 1.875 in.

ΔP_v (in. Hg)	h (in.)	$\sqrt{\Delta P_v}$	$P_{chamber}$ $(h - h_{zero})$
3.02	1.7240	1.74	− .1010
3.10	1.7661	1.76	− .0589
3.18	1.7858	1.78	− .0352
3.29	1.8213	1.81	− .0037
3.30	1.8350	1.82	.0100
3.48	1.8797	1.86	.0547
3.56	1.9068	1.89	.0918

h_{zero} = 1.8250 in.

ΔP_v = pressure drop across venturi

h = Micromanometer reading for pressure
difference across orifice

TABLE XXIX

Entrainment Data

86

STEADY FLOW

AXIAL STATION: 7.75 in.

ORIFICE DIAMETER: 1.875 in.

ΔP_v (in. Hg)	h (in.)	$\sqrt{\Delta P_v}$	$P_{chamber}$ $(h - h_{zero})$
2.30	1.1508	1.52	- .6743
2.75	1.6123	1.66	- .2128
2.85	1.6796	1.69	- .1455
2.92	1.7278	1.71	- .0973
3.00	1.7915	1.73	- .0336
3.02	1.8365	1.74	.0114
3.16	1.9047	1.79	.0796
3.19	1.9348	1.79	.1097

h_{zero} = 1.8251 in.

ΔP_v = pressure drop across venturi

h = Micromanometer reading for pressure
difference across orifice

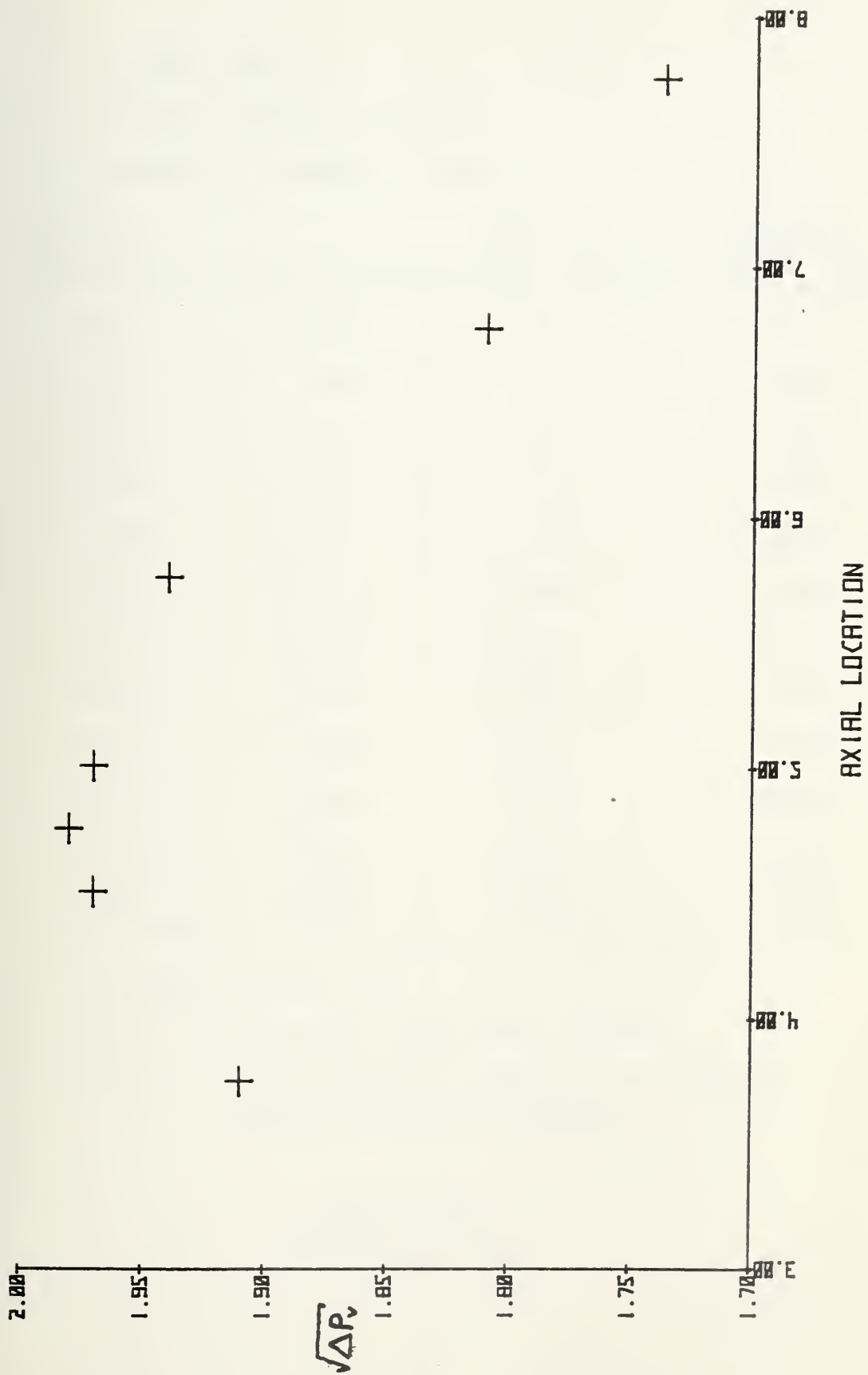TABLE XXX

Entrainment Data

Figure 31. $\sqrt{P_v}$ for zero pressure gradient vs axial location

STEADY FLOW

AXIAL STATION: 4.25 in.

ORIFICE DIAMETER: 1.875 in.

ΔP_v (in.)	h (in.)	$\sqrt{\Delta P_v}$ (in.)	$P_{chamber}$ $(h - h_{zero})$
25.32	1.7184	5.03	- .1134
25.91	1.7536	5.09	- .0782
26.17	1.7875	5.12	- .0443
26.30	1.8012	5.13	- .0306
26.46	1.8132	5.14	- .0186
26.60	1.8276	5.16	- .0042
26.67	1.8172	5.16	- .0146
26.93	1.8517	5.19	.0199
27.10	1.8635	5.21	.0317
27.12	1.8542	5.21	.0224
27.40	1.8903	5.23	.0585
27.70	1.9091	5.26	.0773

h_{zero} = 1.8318 in.

ΔP_v = pressure drop across venturi

h = Micromanometer reading for pressure difference across orifice

TABLE XXXI

Entrainment Data

STEADY FLOW

AXIAL STATION: 4.50 in.

ORIFICE DIAMETER: 1.875 in.

ΔP_v (in.)	h (in.)	$\sqrt{\Delta P_v}$ (in.)	$P_{chamber}$ $(h - h_{zero})$
25.60	1.6717	5.06	- .1601
25.95	1.7223	5.09	- .1095
26.20	1.7467	5.12	- .0851
26.25	1.7628	5.12	- .0690
26.45	1.7946	5.14	- .0372
26.55	1.7891	5.15	- .0427
27.17	1.8431	5.21	.0113
27.45	1.8435	5.24	.0117
27.60	1.8515	5.25	.0197
27.70	1.8788	5.26	.0470
27.95	1.9042	5.29	.0724

h_{zero} = 1.8318 in.

ΔP_v = pressure drop across venturi

h   = Micromanometer reading for pressure
          difference across orifice

TABLE XXXII

Entrainment Data

90

STEADY FLOW

AXIAL STATION: 4.75 in.

ORIFICE DIAMETER: 1.875 in.

ΔP_v (in.)	H (in.)	$\sqrt{\Delta P_v}$ (in.)	$P_{chamber}$ $(h - h_{zero})$
25.90	1.7338	5.09	- .0980
26.00	1.7338	5.10	- .0980
26.10	1.7678	5.11	- .0640
26.40	1.7742	5.14	- .0576
26.55	1.7869	5.15	- .0449
26.70	1.8119	5.17	- .0199
26.75	1.8374	5.17	.0056
26.85	1.8183	5.18	- .0135
27.15	1.8436	5.21	.0118
27.30	1.8513	5.22	.0195
27.65	1.8953	5.26	.0635
27.70	1.8671	5.26	.0353
28.00	1.9248	5.29	.0930

h_{zero} = 1.8318

ΔP_v = pressure drop across venturi

h = Micromanometer reading for pressure difference across orifice

TABLE XXXIII

Entrainment Data

91

STEADY FLOW

AXIAL STATION: 4.25 in.

ORIFICE DIAMETER: 1.875 in.

ΔP_v (in.)	h (in.)	$\sqrt{\Delta P_v}$ (in.)	$P_{chamber}$ (h - h_{zero})
26.70	1.8577	5.17	.0165
26.85	1.8528	5.18	.0116
26.95	1.8512	5.19	.0100
27.10	1.8595	5.21	.0183
27.20	1.8531	5.22	.0119
27.35	1.8524	5.23	.0112

h_{zero} = 1.8412 in.

ΔP_v = pressure drop across venturi

h   = Micromanometer reading for pressure
      difference across orifice

TABLE XXXIV
Entrainment Data

92

STEADY FLOW

AXIAL STATION: 4.50 in.

ORIFICE DIAMETER: 1.875 in.

ΔP_V (in.)	h (in.)	$\sqrt{\Delta P_V}$ (in.)	$P_{chamber}$ $(h - h_{zero})$
26.40	1.8671	5.14	.0118
26.50	1.8650	5.15	.0097
26.60	1.8690	5.16	.0137
26.80	1.8680	5.18	.0127
26.95	1.8707	5.19	.0154
27.20	1.8671	5.22	.0118

h_{zero} = 1.8553 in.

ΔP_V = pressure drop across venturi

h = Micromanometer reading for pressure difference across orifice

TABLE XXXV

Entrainment Data

STEADY FLOW

AXIAL STATION: 4.75 in.

ORIFICE DIAMETER: 1.875 in.

ΔP_v (in.)	h (in.)	$\sqrt{\Delta P_v}$	$P_{chamber}$ $(h - h_{zero})$
26.30	1.8546	5.13	.0141
26.45	1.8616	5.14	.0211
26.55	1.8579	5.15	.0174
26.70	1.8567	5.17	.0162
26.85	1.8547	5.18	.0142
26.90	1.8554	5.19	.0149

h_{zero} = 1.8405

ΔP_v = pressure drop across venturi

h   = Micromanometer reading for pressure
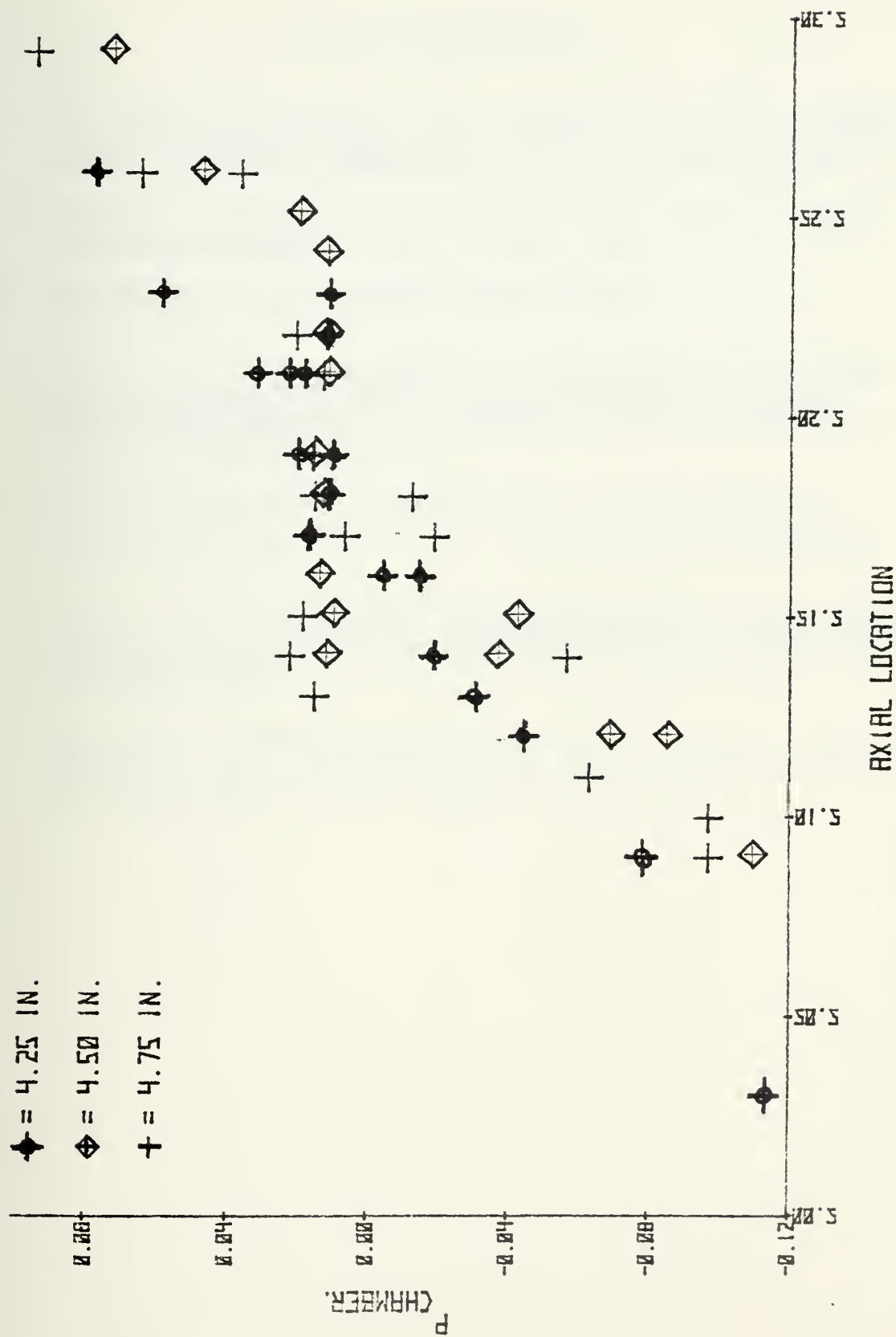   difference across orifice

TABLE XXXVI

Entrainment Data

94

Figure 32. Chamber pressure vs axial location

LIST OF REFERENCES

1. Rockwell International Final Report NR75H-129, <u>A Study of Potential Techniques for Increasing Jet Entrainment Rates in Ejector Augmentors</u>, by E.F. Schum, October 1975.

2. Aerospace Research Laboratories Report 75-0224, <u>Thrust Augmenting Ejectors</u>, by H. Viets, June 1975.

3. Schlichting, H., <u>Boundary Layer Theory</u>, p. McGraw Hill, 1960.

4. Hollis, M.K., <u>Measurement of Instantaneous Velocities From a Fluidically Controlled Nozzle Using a Laser Doppler Velocimeter</u>. M.S. Thesis, Naval Postgraduate School, Monterey, 1976.

5. Ricou and Spalding, "Measurement of Entrainment by Axisymmetric Turbulent Jets," <u>Jo. of Fluid Mechanics</u>, Volume 11, 1971.

6. Weiss, D.L., <u>An Experimental Investigation of the Whistler Nozzle and an Analytical Investigation of a Ring Wing in Supersonic Flow</u>, M.S. Thesis, Naval Postgraduate School, Monterey, 1976.

7. Aerospace Research Laboratories Report 74-0113, <u>Development of a Time Dependent Nozzle</u>, by H. Viets, July 1974. Also published in AIAA Journal, October 1975, p. 1375-1379.

INITIAL DISTRIBUTION LIST

		No. Copies
1.	Defense Documentation Center Cameron Station Alexandria, Virginia 22314	2
2.	Library, Code 0212 Naval Postgraduate School Monterey, California 93940	2
3.	Chairman, Aeronautics Department, Code 67Be Naval Postgraduate School Monterey, California 93940	1
4.	Professor M.F. Platzer, Code 67Pl Department of Aeronautics Naval Postgraduate School Monterey, California 93940	5
5.	LT Richard James Veltman Route 1, Box 292 Easton, Maryland 21601	1
6.	Dr. H.J. Mueller Research Administrator Code AIR-310 Naval Air Systems Command Washington, D.C. 20360	1